

~~CONFIDENTIAL~~Copy  
RM E52I15

NACA RM E52I15

**NACA**

014333

TECH LIBRARY KAFB, NM



# RESEARCH MEMORANDUM

6774

## PERFORMANCE CHARACTERISTICS OF SEVERAL TYPES OF AXIALLY SYMMETRIC NOSE INLETS AT MACH NUMBER 3.85

By James F. Connors and Richard R. Woollett

Lewis Flight Propulsion Laboratory

Unclassified Cleveland, Ohio

NACA Tech Pub Announcement #4

16 Mar. 59

NK .....

**RECEIPT SIGNATURE  
REQUIRED**

GRADE OF OFFICER MAKING CHECK

14 Mar. 61

DATE

CLASSIFIED DOCUMENT

This material contains information affecting the National Defense of the United States within the meaning of the espionage laws, Title 18, U.S.C., Secs. 793 and 794, the transmission or revelation of which in any manner to unauthorized persons is prohibited by law.

## NATIONAL ADVISORY COMMITTEE FOR AERONAUTICS

WASHINGTON

November 13, 1952

314.98/13

~~CONFIDENTIAL~~



0143330

1Y

NACA RM E52I15

## NATIONAL ADVISORY COMMITTEE FOR AERONAUTICS

RESEARCH MEMORANDUMPERFORMANCE CHARACTERISTICS OF SEVERAL TYPES OF AXIALLY  
SYMMETRIC NOSE INLETS AT MACH NUMBER 3.85

27794

By James F. Connors and Richard R. Woollett

## SUMMARY

An experimental investigation was conducted at a Mach number of 3.85 to determine the diffuser characteristics of a series of conventional axially symmetric nose inlets mounted on a 5-inch ram jet in the Lewis 2- by 2-foot supersonic wind tunnel. Performance evaluations of single-cone, double-cone, and isentropic diffusers were made in terms of total-pressure recovery and mass flow for a range of angles of attack from 0° to 10°; in addition, cowl pressure distributions were obtained at zero angle of attack.

At zero angle of attack the single-cone, double-cone, and isentropic diffusers yielded total-pressure recoveries of 0.32, 0.44, and 0.57 with corresponding supercritical mass-flow ratios of 0.995, 0.94, and 0.905, respectively. A maximum total-pressure recovery of 0.625, corresponding to a kinetic-energy efficiency of 95 percent, was obtained with an isentropic inlet utilizing boundary-layer removal through a permeable wall centerbody. Improvements in inlet performance were realized with the application of tip roughness to reduce boundary-layer separation on both the 2-cone and the isentropic inlets and also with the application of suction to modify a local flow separation occurring immediately downstream of a sharp turn on the 1-cone (low-angle cowl) inlet. None of the inlets (all of which were designed for conical-shock interception with the cowl lip) exhibited any stable range of subcritical operation.

Based on specific fuel consumption or range considerations for hypothetical ram-jet engines, a comparison of the various inlets at zero angle of attack showed that the 1-cone (low-angle cowl), the 2-cone (tip roughness), and the isentropic (with minimum additive drag based on the assumption of supersonic flow spillage) inlets were competitive with one another. However, use of the higher recovery inlets to produce a given amount of thrust minus drag would result in smaller engine sizes.

~~CONFIDENTIAL~~

## INTRODUCTION

A comprehensive survey of the literature was made to ascertain the current status of existing diffuser data over the supersonic speed range. For Mach numbers below approximately 3.1, it was found that rather extensive research on diffuser pressure recovery and mass-flow characteristics had been conducted and that diffusers capable of yielding peak total-pressure recoveries corresponding to kinetic-energy efficiencies of 95 percent appeared to be fairly representative of the upper limit of performance. At Mach numbers greater than 3.1, however, only limited inlet data appeared available.

2644

Since from the standpoint of missile application there exists considerable interest in the higher Mach number range, an experimental diffuser program was undertaken at a Mach number of 3.85 at the NACA Lewis laboratory. The purpose of the investigation was (1) to experimentally evaluate the performance characteristics of several conventional axially symmetric nose inlets of the single- and multiple-oblique-shock variety, (2) to explore any possible gains in performance which may be obtained by controlling or modifying the boundary layers encountered along the compression surfaces, and (3) to indicate an over-all performance comparison of the various specific inlet configurations that were to be studied.

Accordingly, cold-flow experiments were conducted on a series of inlets mounted on a 5-inch ram jet. These diffuser configurations consisted basically of axially symmetric inlets having (1) a single conical compression surface with no internal contraction, (2) a single conical compression surface with a variable internal contraction, (3) two conical compression surfaces with the maximum allowable internal contraction, and (4) a continuously curving (isentropic) compression surface with no internal contraction. In order to investigate the effectiveness of several boundary-layer control schemes, provisions were incorporated in the designs to permit the application of either local or distributed wall suction on the diffuser centerbodies. Performance characteristics in terms of total-pressure recovery and mass flow were obtained at a Mach number of 3.85 over a range of angles of attack from  $0^\circ$  to  $10^\circ$ ; cowl pressure distributions were obtained at zero angle of attack. Preliminary force measurements obtained with a strain-gage balance system essentially verified the order of magnitude of the estimated drags which are presented herein; however, enough experimental scatter existed in the force data to preclude their presentation in this first report. Some of the data reported herein have also been included in a preliminary survey report on high Mach number diffusers (reference 1).

## SYMBOLS

The following symbols are used in this report:

A	local flow area, sq ft
$A_{max}$	maximum frontal area of engine, sq ft
$C_{D,C}$	cowl pressure-drag coefficient, $D_C/q_0 A_{max}$
$C_{D,E}$	external-drag coefficient, $D_E/q_0 A_{max}$
$C_p$	static-pressure coefficient, $2(p_x - p_0)/\gamma p_0 M_0^2$
$D_C$	cowl pressure drag, lb
$D_E$	total external drag, lb
$M_0$	free-stream Mach number
$m_3$	mass-flow rate through engine, slugs/sec
$m_{max}$	mass-flow rate through a free-stream-tube area equal to maximum capture area of inlet, slugs/sec
$P_0$	free-stream total pressure, lb/sq ft
$P_3$	diffuser-exit total pressure, lb/sq ft
$p_x$	local static pressure, lb/sq ft
$p_0$	free-stream static pressure, lb/sq ft
$q_0$	free-stream dynamic pressure ( $\gamma p_0 M_0^2/2$ ), lb/sq ft
$R_L$	cowl lip radius, ft
$R_{max}$	engine radius, ft
sfc	specific fuel consumption, lb fuel/(lb thrust)(hr)
$\alpha$	angle of attack, deg
$\gamma$	ratio of specific heats
$\eta_{K.E.}$	kinetic energy efficiency defined as ratio of kinetic energy available after diffusion to kinetic energy in the free stream,

$$1 - \frac{2}{(\gamma-1)M_0^2} \left[ \left( \frac{P_0}{P_3} \right)^{\frac{\gamma-1}{\gamma}} - 1 \right]$$

## APPARATUS AND PROCEDURE

The experimental investigation was conducted in the NACA Lewis 2- by 2-foot supersonic wind tunnel at a Mach number of 3.85 and at a simulated pressure altitude of 108,000 feet. The tunnel air was maintained at a temperature of  $200^{\circ} \pm 5^{\circ}$  F and at a dew-point temperature of  $-15^{\circ} \pm 10^{\circ}$  F. Based on the maximum diameter of the engine (5 inches), the test Reynolds number was approximately 429,000.

The basic model and support system are represented schematically in figure 1(a) and photographically in figure 1(b). As illustrated, the 5-inch ram-jet engine was sting mounted to the tunnel support system and was equipped with a variable-exit plug which was utilized to vary the inlet back pressure. In order to provide a means of applying suction to the boundary layer along the compression surfaces, the centerbody of the ram jet was vented to the free-stream static pressure through three hollow support struts. Provisions were also available for collecting and measuring the bledoff mass flow through the use of a manifold and rotameter arrangement. The tunnel strut permitted an angle-of-attack variation on the model of approximately  $11^{\circ}$  measured from the zero angle-of-attack condition. At the front end of the model, inlet configurations, consisting of interchangeable spikes and cowls, were installed.

Design details of the various inlets are presented in table I, in the drawings of figure 1(c), and in the photographs of figure 1(d). The l-cone inlet had a vertex angle of  $60^{\circ}$ , which approximated the optimum diffusion angle on the basis of theoretical shock losses. No internal contraction was employed and the cowl lip was located so as to just intercept the conical shock. The internal passage was designed for an arbitrary gradual turning of the flow back toward the axial direction with the cowl lip initially arranged in the direction of the flow immediately behind the conical shock.

A variation of the above diffuser was the l-cone (low-angle cowl) inlet, which was designed to represent an extreme case by employing a sharp rapid turning of the flow in order to obtain a near minimum projected frontal area and thereby a low pressure drag on the cowl. With this design, then, a strong compression wave would originate internally at the cowl lip. Subsequent results necessitated the application of local suction through a double row of staggered  $1/8$ -inch-diameter holes located immediately downstream of the sharp turn. The cone vertex angle was again  $60^{\circ}$  and a slight internal contraction existed as a result of the cylindrical internal surface of the cowl.

A combination of both external and internal compression was used on the l-cone (variable internal contraction) inlet. On design position, the shock from the tip of the  $40^{\circ}$  cone just intercepted the cowl lip and the internal contraction was such that from unidimensional flow considerations the stream Mach number would then be reduced to 1.40 at the throat.

In order not to exceed the starting limitation (reference 2), provisions were incorporated in the design to move the cone forward and thereby reduce the internal contraction. Once the shock was swallowed, the cone was then retracted towards the design position.

Another configuration, designated the 2-cone inlet, employed two conical surfaces to generate the desired compression waves. The shocks, emanating from the  $40^{\circ}$  initial cone angle and the  $70^{\circ}$  secondary cone angle, were designed to intercept the cowl lip. Internally, the flow passages were designed for the maximum allowable internal contraction ratio, corresponding to an estimated average entrance Mach number. Later experimental refinements involved the use of tip roughness in the form of a 1/2-inch band of (number 60) carborundum grit and also the application of local suction through a double row of staggered 1/8-inch-diameter holes located just upstream of the juncture between the two conical surfaces.

The isentropic inlet which theoretically employed an infinite number of very weak compression waves was designed by the method of characteristics (reference 3). The resulting configuration consisted of a center spike with a continuously curving surface to generate the desired compression with the focal point of the characteristics located at the cowl lip and with a final Mach number of the flow equal to 1.5 at the diffuser entrance. An initial cone angle of  $16^{\circ}$  was arbitrarily selected. There was no internal contraction and the cowl lip was designed to receive the internal flow initially in the stream direction with the result that the external angle of the cowl lip exceeded the detachment angle corresponding to the free-stream Mach number. Experiments were also made on this inlet with the use of tip roughness (a 1/2-inch band of number 60 carborundum grit). Another variation of the isentropic inlet included the use of a porous center spike fabricated out of sintered bronze. The relations given in reference 4 were used to determine an order of magnitude of the suction that might be required on such a configuration. Then, porosity and wall thickness were calculated with the use of sintered-bronze calibration charts given in a commercial catalog. However, the porosity of the actual model was not experimentally verified. After preliminary experiments, it was found that better results were obtained after the porous section downstream of the throat had been sealed off with lacquer. This technique appeared to give better control of the boundary layer on the upstream compression surface. In later tests at positive angles of attack, the effect of sealing off the pores on the entire lower half of the spike was also studied.

Internal area distributions along the axis of the diffuser, measured from the plane of the cowl lip to the constant-area section at the diffuser outlet, are presented for the original inlet configurations in figure 1(e). As shown, the major portion of the subsonic or divergent

passage (starting at the 0-station) was common to all the inlets and was designed to yield an approximate 5°-conical-area expansion. The curves showing the area variations forward of this section for the different inlets were then faired into the common curve. Internal contraction was incorporated in both the 1-cone (low-angle cowl) and the 2-cone inlets.

Pressure instrumentation consisted of a total- and static-pressure rake (fig. 1(f)) located at the diffuser exit and three longitudinal rows (top, side, and bottom) of wall statics located on each inlet cowl for measuring external pressure distributions. The total pressures at the diffuser exit were obtained by an area weighting of the pitot-rake pressures. From measurements of the sonic discharge area and the static pressure at the rake, mass-flow rates were computed with the assumption of one-dimensional flow. Cowl pressure drags were obtained from integrations of the external pressure distributions.

Complete pressure data were recorded over a wide range of exit-plug positions at angles of attack from 0° to 10°.

2644

#### RESULTS AND DISCUSSION

In the following discussion, the designation of the 1-cone, the 2-cone, and the isentropic inlets will refer to the configurations as originally designed and as described earlier. Unless otherwise specified, the designation 1-cone (low-angle cowl) inlet will include the use of suction holes downstream of the throat on the previously described inlet configuration. Other modifications to the original designs (such as the use of tip roughness, the application of suction, the use of an extended or retracted cowl, etc.) will always be included parenthetically in the designation of the particular inlets.

#### Performance of 1-Cone Inlets

Diffuser characteristics of the 1-cone inlet are presented in figure 2(a) for several angles of attack. At zero angle of attack a maximum total-pressure recovery  $P_3/P_0$  of 0.315 (compared to a theoretical shock-loss value of 0.36) was attained with a corresponding supercritical mass-flow ratio of 0.95. By extending the cowl 1/16 inch forward of its design position, the supercritical mass-flow ratio  $m_3/m_{\max}$  was increased to nearly 1.00 with the conical shock from the tip appearing from schlieren observations to fall inside the diffuser. With this increase in mass flow the maximum recovery value remained unchanged. Because this diffuser definitely appeared to capture the maximum free-stream tube of air, the 1-cone (extended cowl) inlet provided the sole experimental check on the accuracy of the mass-flow calculations. The

fact that the supercritical mass-flow ratio fell so close to unity (0.993) may have been somewhat fortuitous, however, since later tests on other configurations with the conical shock inside the cowl showed mass-flow ratios 2 to 3 percent less than 1.00. No calibration or correction factor was employed in the present mass-flow computations. As the angle of attack of the inlet was increased to  $9^\circ$ , both pressure recovery and mass flow were found to decrease. At all attitudes, it was observed that there was no stable subcritical operation and that "buzz" or pulsing flow occurred immediately upon expulsion of the diffuser shock.

A modification aimed at achieving a low-drag cowl was incorporated in the design of the 1-cone (low-angle cowl) inlet. The performance characteristics of this diffuser are shown in figure 2(b). Initial experiments at zero angle of attack indicated a detached shock wave ahead of the cowl lip and boundary-layer separation along the cone surface with a resultant low-pressure recovery and a large amount of flow spillage, as shown in the figure. Failure of the diffuser to swallow the shock was attributed to a local flow separation occurring immediately downstream of the sharp turn on the centerbody. Such a separation could presumably be caused by an adverse pressure gradient in the divergent passage downstream of the throat and could result in an internal contraction of the flow in excess of the Kantrowitz-Donaldson limiting value (reference 2). To overcome this starting difficulty, suction was applied through a double row of circular holes just downstream of the sharp turn. (The use of suction to reduce flow separation near the diffuser throat was qualitatively demonstrated in reference 5). As indicated by the data, the diffuser shock was swallowed and at zero angle of attack the following results were obtained: maximum total-pressure recovery of 0.32, a critical total-pressure recovery of 0.30, and a supercritical mass-flow ratio of 0.925. Measurements of the bleed flow during supercritical operation showed that approximately 1 percent of the maximum capture mass flow  $m_{max}$  was required in the suction process. An attempt to increase the supercritical mass-flow ratio by extending the cowl  $1/32$  inch forward of its design position again resulted in a detached shock at the entrance of the diffuser. Angle-of-attack performance with suction is also included in figure 2(b).

Another configuration, the 1-cone (variable internal contraction) inlet, was designed for both external and internal compression. As will be shown in subsequent photographs, boundary-layer separation, due to pressure feedback, occurred in the convergent passage and along the cone surface upstream of the entrance of the diffuser. The application of suction locally on the compression surface served to change the separation pattern and to permit the attainment of larger values of geometric contraction ratio than in the no-suction case. However, the diffuser performance data showed no advantage for either arrangement, both with and without suction a maximum total-pressure recovery of 0.25 was obtained at zero angle of attack with a corresponding mass-flow ratio of

approximately 0.3. The use of a porous-wall centerbody to provide a distributed suction also gave similar results to that obtained in the no-suction case. Thus, on this particular variable-geometry arrangement, the attainment of large amounts of internal compression was prevented by a separation of the boundary layer in the convergent passage and no improvement in diffuser performance could be obtained by the addition of either local or distributed suction.

The effects of angle of attack on the performance of the l-cone inlets are summarized in figure 3. In general, the curves, showing the decrease of maximum pressure recovery and supercritical mass-flow ratio with angle of attack for both the l-cone and the l-cone (low-angle cowl) inlets, are quite similar with each having approximately the same slope although located on different levels. Over the 10°-angle-of-attack range the total-pressure recovery of the l-cone (low-angle cowl) inlet was slightly higher (2 percent) and the supercritical mass-flow ratio 2.5 to 6 percent lower than corresponding values of the l-cone inlet.

Schlieren photographs of the shock-wave patterns obtained with the l-cone inlets at zero and 9° angles of attack are presented in figure 4. On the l-cone inlet (fig. 4(a)) the conical shock from the tip very nearly intercepted the cowl lip at zero angle of attack. At 9° angle of attack, increased spillage is indicated by the tip shock being located ahead of the cowl lip. At the same time the boundary layer was observed to wash toward the leeward side of the cone and thus produce a thickening of the boundary layer on the top with some thinning on the bottom due to body cross-flow effects. For the l-cone (low-angle cowl) inlet with no suction (fig. 4(b)), a detached shock stood ahead of the cowl with boundary-layer thickening upstream thereof. With the application of suction the diffuser shock was swallowed and the conical shock from the tip nearly intercepted the cowl lip. At 9° angle of attack a detached shock was formed at the lower lip, otherwise the pattern was similar to that of the l-cone inlet. The shock-wave patterns obtained with the l-cone (variable internal contraction) inlet are presented in figure 4(c). The photographs on the left and on the right show the shock configurations obtained with the cone at the minimum (stable flow) tip projection for no suction and for local suction, respectively. With no suction, a well defined separation of the boundary layer occurred just ahead of the inlet. With local suction on the cone, the flow appeared to separate at a much steeper angle with an accompanying stronger shock system. For values of tip projection smaller than the preceding minimums, the inlet flow pattern was characterized by high-frequency oscillations of the flow, as evidenced by the blurred pattern in the center photograph of figure 4(c).

2644  
Performance of 2-Cone Inlets

The performance of the 2-cone inlet is presented in figure 5(a), where total-pressure recovery  $P_3/P_0$  is again plotted as a function of mass-flow ratio  $m_3/m_{\max}$ . At zero angle of attack a maximum total-pressure recovery of 0.41 (compared to a theoretical shock-loss value of 0.61) was obtained with a corresponding mass-flow ratio of 0.855. As will be illustrated in later photographs, the boundary layer was observed to separate and effectively bridge the juncture of the two conical compression surfaces. This particular diffuser was found to exhibit a rather unusual variation of supercritical mass-flow ratio with angle of attack. With increasing angle of attack the supercritical mass-flow ratio increased to a maximum at approximately  $4^\circ$  and then decreased with further increases in angle of attack. This variation is associated with the boundary-layer bridging at the break between the two cones. Apparently at the smaller angles of attack ( $\alpha < 4^\circ$ ) the boundary layer was favorably modified by the body cross flow so that the gain resulting from the wiping action on the boundary layer at the bottom more than offset the effect of increased bridging at the top. At  $9^\circ$  angle of attack a hysteresis loop in the curve was encountered. At this attitude, subcritical operation of the inlet was characterized by large-scale separation of the flow from the upper half of the cone. The corresponding flow pattern appeared to be nearly steady although a slightly blurred shock was observed in the schlieren photograph. In order to reset conditions for supercritical operation, it was necessary to reduce the diffuser back pressure considerably below the critical value, thereby establishing the hysteresis loop. At the lower angles of attack on figure 5(a), the inlet exhibited the usual subcritical buzz characteristics.

On figure 5(b) the performance characteristics of the 2-cone (extended cowl) inlet are presented for several angles of attack. A maximum total-pressure recovery of 0.435 with a corresponding mass-flow ratio of 0.91 was realized at zero angle of attack. Because of the added cowl extension (1/16 inch), the increase in pressure recovery is attributed to the resultant slight increase in internal contraction above that of the 2-cone inlet (fig. 5(a)). At angles of attack of  $3^\circ$  and  $5\frac{1}{2}^\circ$ , the flow separated on the top half of the cone during subcritical operation and could not be reattached except by decreasing the angle of attack with a reduced inlet back pressure and then resetting the desired  $\alpha$ . At  $9^\circ$  angle of attack this type of separation pattern persisted under all inlet operating conditions.

Roughness was applied to the tip of the 2-cone inlet in an attempt to artificially induce transition to a turbulent boundary layer. The performance of the 2-cone (tip roughness) inlet is given in figure 5(c) for several angles of attack. A maximum total-pressure recovery of 0.445

was obtained with a supercritical mass-flow ratio of 0.94 at zero angle of attack. As will be shown in subsequent schlieren photographs, the boundary-layer bridging at the juncture of the two conical surfaces was markedly reduced. The improvement in inlet performance was the result of simulating an effective change in Reynolds number by the addition of tip roughness designed to promote premature transition. In addition, the unusual mass-flow variation with angle of attack previously described for the 2-cone and 2-cone (extended cowl) inlets was eliminated. Both total-pressure recovery and mass-flow ratio decreased with increasing angle of attack up to approximately  $8\frac{1}{2}^{\circ}$ , above which the flow separated from the upper half of the cone.

The effect of angle of attack on the performance of the various 2-cone inlets are summarized in figure 6. The 2-cone (tip roughness) inlet avoided the unusual mass-flow variation associated with boundary-layer bridging at the break and yielded the best performance of the three diffusers for angles of attack up to  $8\frac{1}{2}^{\circ}$ , where the discontinuity occurred in the curves because of flow separation. For operation over the entire range, the 2-cone inlet was the only one that did not incur the discontinuity due to separation.

Another configuration that was investigated was the 2-cone (suction) inlet, which employed suction locally just upstream of the juncture between the two conical surfaces to prevent local separation. No data are presented for this inlet since it can be simply stated that similar results were obtained as with the 2-cone (tip roughness) inlet (fig. 6) but with the range of angle-of-attack operation without flow separation increased to slightly less than  $11^{\circ}$ .

Typical schlieren photographs of the flow patterns obtained with the 2-cone inlets are presented in figure 7 for zero and  $9^{\circ}$  angles of attack. With the 2-cone inlet (fig. 7(a)) extensive boundary-layer bridging can be observed at the juncture of the two cones at zero angle of attack. With the inlet at  $9^{\circ}$ , there was a pronounced thinning of the boundary-layer bridge on the bottom with increased thickness on the top. The effect of tip roughness on the boundary layer at zero angle of attack is clearly illustrated in figure 7(b), where it can be seen that the boundary-layer bridging had been virtually eliminated. At  $9^{\circ}$  angle of attack the flow had completely separated from the upper half of the cone. This pattern was typical of those previously described as having flow separation on the top of the cone. With each of the 2-cone inlets at  $9^{\circ}$  angle of attack, a detached shock was formed ahead of the cowl lip on the bottom.

~~CONFIDENTIAL~~

### Performance of Isentropic Inlets

The diffuser characteristics of the isentropic inlet are presented for several angles of attack in figure 8(a). At zero angle of attack, a maximum total-pressure recovery of 0.57 (compared with a theoretical shock-loss value of 0.93) was obtained with a corresponding supercritical mass-flow ratio of 0.905. At the same time schlieren observations revealed a separation of the laminar boundary layer along the compression surface with subsequent reattachment of the flow. Both pressure recovery and mass-flow ratio were found to decrease with increasing angle of attack. However, at an angle of attack of  $9^{\circ}$  a large separation of the flow was observed on the upper half of the spike. Over the angle-of-attack range investigated, there was no evidence of any stable subcritical operation.

In an attempt to artificially induce transition to a turbulent boundary layer which would be more resistant to flow separation, tip roughness was again employed on the above inlet. The results obtained with this isentropic (tip roughness) inlet are given in figure 8(b) for several angles of attack. A maximum total-pressure recovery of 0.615 was obtained at zero angle of attack with a supercritical mass-flow ratio of 0.87. In general, the curves show the usual decreasing values of maximum pressure recovery and supercritical mass-flow ratio with increasing angle of attack. At  $9.1^{\circ}$  angle of attack some oscillation of the shock pattern was observed to occur on the top half of the spike.

Another configuration which employed a distributed suction through a permeable centerbody wall was designed to avoid any separation of the boundary layer due to the influence of the strong adverse pressure gradients. The results obtained with this isentropic (porous, retracted cowl) inlet are presented for zero angle of attack in figure 8(c). The maximum total-pressure recovery of 0.625, corresponding to a kinetic-energy efficiency  $\eta_{K.E.}$  of 95.2 percent, was the highest obtained in the present investigation and was obtained with a supercritical mass-flow ratio of 0.82. The maximum amount of mass flow removed through the porous spike was approximately 1.5 to 2 percent of the mass flow entering the diffuser.

In preliminary experiments with this configuration at angle of attack, it appeared that the effect of suction on the boundary layer along the upper half of the spike had been greatly reduced from that observed at zero angle of attack. Therefore, in an attempt to maintain a concentrated suction on the upper half of the spike, where the extent of any flow separation would be the greatest at positive angles of attack, the lower half of the porous spike was sealed off with lacquer. The performance characteristics of this isentropic (half porous, retracted cowl) inlet are presented in figure 8(c). At zero angle of attack a maximum total-pressure recovery of 0.58 was obtained with a

supercritical mass-flow ratio of 0.83. There was no evidence of flow separation over the entire angle-of-attack range. In each case, there was no stable subcritical operation.

With the difference in supercritical mass-flow ratios at zero angle of attack between 0.905 for the isentropic inlet and 0.83 for the isentropic (half porous, retracted cowl) inlet, it was difficult to weigh the contribution of suction to the increased angle-of-attack range realized with the half-porous configuration. Therefore, the cowl on the isentropic inlet was similarly retracted (1/32 inch) to deliberately incur additional flow spillage at  $\alpha = 0^\circ$ . The diffuser characteristics of the isentropic (retracted cowl) inlet are shown in figure 8(d). A maximum pressure recovery of 0.56 was obtained at  $\alpha = 0^\circ$  with a supercritical mass-flow ratio of 0.82. As illustrated, no separation was encountered within the  $9^\circ$ -angle-of-attack range. Apparently, this increased range of angle-of-attack operation without separation on the upper half of the spike was associated with the decrease in the  $\alpha = 0^\circ$  mass-flow ratio rather than with the application of suction as on the half-porous configuration. However, the higher level of pressure recovery, obtained over the entire angle-of-attack range with the isentropic (half porous, retracted cowl) inlet when compared with the isentropic (retracted cowl) inlet, seemed to warrant the presentation of this performance data.

2644

Summary curves illustrating the relative performance of the isentropic inlets over the angle-of-attack range are presented in figure 9. In general, all the isentropic inlets exhibited a larger rate of decrease in pressure recovery with increasing angle of attack than either the 1-cone or 2-cone inlets; however, the isentropic inlets were still superior in terms of pressure recovery for angles of attack up to approximately  $6^\circ$ . As evidenced by the isentropic (half-porous, retracted cowl) and the isentropic (retracted cowl) inlets, it also appeared that, by accepting a decrease in the  $\alpha = 0^\circ$  mass-flow ratio, the range of angle-of-attack operation without flow separation could be extended to larger angles.

Typical schlieren photographs of the inlet shock-wave patterns are presented for zero and approximately  $9^\circ$  angles of attack in figure 10. At zero angle of attack, thick boundary-layer bridging was observed on the solid isentropic spikes with smooth tips in figures 10(a) and 10(d). With the application of roughness (fig. 10(b)) or distributed suction (fig. 10(c)) the thickness of the observed boundary layer was markedly reduced. Similar observations were made in two-dimensional isentropic inlet studies (reference 6). This observed pattern of boundary-layer bridging is regarded as a separation of the laminar boundary layer followed by reattachment. The action of the roughness in avoiding such separation was presumably to trigger an initially turbulent boundary layer. All the isentropic inlets appeared to have a detached shock at

the cowl lip and some attendant flow spillage. At  $9^{\circ}$  angle of attack the flow separated on the upper half of the spike for both the isentropic inlet (fig. 10(a)) and the isentropic (tip roughness) inlet (fig. 10(b)). With all the inlets a large bow wave stood ahead of the cowl on the lower half of the spike and, just upstream of this, the envelope of compression waves formed a curved shock pattern.

#### EXIT TOTAL-PRESSURE PROFILES

Total-pressure distributions at the diffuser exit during critical engine operation are presented in figure 11 for the 1-cone (low-angle cowl), the 2-cone, and the isentropic inlets at several angles of attack. All the inlets exhibited flat and uniform profiles at zero angle of attack. At positive angles of attack all the inlets indicated some flow separation in the lower quadrant with the sole exception of the isentropic inlet at  $\alpha = 3^{\circ}$ , which for some unknown reason indicated just the opposite with separation occurring in the top quadrant. The isentropic inlet at  $\alpha = 9^{\circ}$  was operating with an inlet shock pattern showing separation of the flow from the upper half of the spike and, correspondingly, the profile appears flat and indicative of extensive flow separation. As expected, higher local discharge velocities generally occurred with the larger angles of attack as indicated by the differential between the local total pressure and the uniform static pressure across the duct.

#### SUBCRITICAL BUZZ OBSERVATIONS

Except for the inlets that had flow separation at the higher angles of attack, all the inlets reported herein indicated no stable subcritical operation with buzz or pulsing flow being initiated immediately upon expulsion of the terminal shock. To illustrate the variation of inlet flow pattern occurring during such a buzz condition, sequences of selected high-speed schlieren photographs are presented in figures 12 and 13 for the 1-cone (low-angle cowl) and the isentropic inlets, respectively, at both zero and positive angles of attack. The pictures were taken at approximately 3000 frames per second and the order of magnitude of the pulse frequency is indicated in the captions on the figure. In general, at zero angle of attack the pulsing seemed to occur in a symmetrical fashion while at angle of attack the pattern was quite different between top and bottom. At positive angles, the normal shock first appeared to move out on the top of the spike and separate the flow out to the tip until a cone aligned with the free-stream direction was formed by the spike and the separation boundary. Then, depending on the amplitude of the pulsing, the shock pattern further developed in an upstream direction and, in some cases, the pattern billowed out to the tip of the spike in a highly irregular manner.

In the present investigation no effort had been made in the design of the inlets to achieve subcritical shock stability. With all the inlet cowl lips designed for conical-shock interception, buzz was to be expected on the basis of the criterion given in reference 7.

### COWL PRESSURE DISTRIBUTIONS

Typical cowl pressure distributions are presented in figure 14 for the four inlet configurations at zero angle of attack and with super-critical engine operation. An integration of these pressures yielded values of cowl pressure drag which are tabulated on the figure in the form of coefficients based on the maximum frontal area of the engine  $A_{max}$ . The cowl with the lowest drag was that of the 1-cone (low-angle cowl) inlet which had a drag coefficient of 0.007. The cowl for the isentropic inlet, which operated with a detached shock at the lip, also had a low value of drag coefficient  $C_{D,C} = 0.056$ , presumably as a result of a large expansion of the spilled flow around the lip due to the large approach angle.

2644

As previously described, buzz or pulsing flow occurred over the entire subcritical operating range. During such a condition, the manometer boards (with the long instrumentation lines which damp out the pulses) tended to read some time-averaged value of the pressures. The drag coefficients, resulting from the integration of such data, showed a decreasing cowl pressure drag with decreasing mass-flow ratio.

### OVER-ALL PERFORMANCE COMPARISON OF THE SPECIFIC INLETS

Calculations were made to obtain comparative performance parameters for the specific inlet configurations applied to hypothetical ram-jet engines operating at zero angle of attack. The results are summarized in the bar graphs of figure 15. Parts (a) and (b) of the figure summarize the maximum total-pressure recoveries and the corresponding mass-flow ratios obtained with the four inlets. A breakdown of the external drag coefficients into their various components is presented in part (c). As discussed previously, the cowl pressure drags were experimentally determined. The friction drags, however, were calculated with the assumption of an average compressible-flow skin-friction coefficient of 0.0013, whereas the additive drags of the 1-cone and 2-cone inlets were estimated by the method of reference 8. Because it was impossible to definitely establish the character of the flow spillage encountered with the isentropic inlet, it was necessary to calculate the two limiting cases of additive drag as follows: (1) A minimum, with the assumption of supersonic flow spillage, was calculated as an integration along a limiting streamline with a pressure distribution taken from a

theoretical solution of the flow field by the method of characteristics, and (2) a maximum was calculated with the assumption of complete momentum loss of the spilled flow. The total drag of the 1-cone (low-angle cowl) inlet was approximately 40 percent lower and the total drag of the isentropic inlet somewhere between 20 and 65 percent higher than that obtained for the 1-cone and 2-cone (tip roughness) inlets.

With use of the values of pressure recovery, mass-flow ratio, and external drag shown in parts (a), (b), and (c), respectively, of figure 15, values of specific fuel consumption were calculated for hypothetical ram-jet engines operating under the following assumed conditions: (1) flight at zero angle of attack, Mach number of 3.85, and an altitude of 80,000 feet; (2) combustion at a fuel-air ratio of 0.024 and a combustion efficiency of 90 percent; and (3) operation with a completely expanded flow through the exit nozzles. The results are presented in part (d) of figure 15. Based on specific fuel consumption or range considerations, a comparison of the four inlets indicated that the 1-cone (low-angle cowl), the 2-cone (tip roughness), and the isentropic (minimum additive drag) inlets were approximately equal and about 14 percent lower than the 1-cone and isentropic (maximum additive drag) inlets.

A relative comparison of these hypothetical ram-jet engines, sized to produce the same thrust minus drag, is shown in part (e) of figure 15. The higher pressure recovery inlets tended to result in smaller engine sizes.

#### SUMMARY OF RESULTS

An experimental investigation of single- and multiple-oblique shock, axially symmetric diffusers yielded the following results at a Mach number of 3.85:

1. A maximum total-pressure recovery of 0.625, corresponding to a kinetic-energy efficiency of 95 percent, was obtained with a porous-spike isentropic inlet at zero angle of attack.
2. Single-cone, double-cone, and isentropic diffusers yielded total-pressure recoveries of 0.32, 0.44, and 0.57 with corresponding supercritical mass-flow ratios of 0.995, 0.94, and 0.905, respectively.
3. On one configuration designated the 1-cone (low-angle cowl) inlet the application of suction immediately downstream of a sharp turn allowed the diffuser shock to be swallowed by modifying a local flow separation and was the means of utilizing an extremely low-drag cowl.

4. The application of tip roughness on the 2-cone and the isentropic inlets appeared to eliminate a separation of the laminar boundary layer and resulted in improved inlet performance at zero angle of attack.

5. The attainment of large amounts of internal compression through the use of a variable-geometry configuration failed because of boundary-layer separation in the convergent passage and no improvement could be obtained by the use of either local or distributed suction.

6. The isentropic inlets, which gave the highest recoveries at zero angle of attack, exhibited a much more pronounced sensitivity to angle-of-attack effects than either the 1-cone or 2-cone inlets. In general, it was found that, by accepting a decrease in the zero angle-of-attack mass-flow ratio, the range of angle-of-attack operation without separation of the flow from the upper half of the spike could be extended to larger angles.

7. No stable subcritical operation was exhibited by any of the inlets, all of which were designed for conical-shock interception of the cowl lip.

8. Based on specific-fuel-consumption considerations, a comparison of the various inlets at zero angle of attack showed that the 1-cone (low-angle cowl), the 2-cone (tip roughness), and the isentropic (minimum additive drag) inlets were competitive with each other. However, use of the higher recovery inlets pointed toward smaller engine sizes to produce a given amount of thrust minus drag.

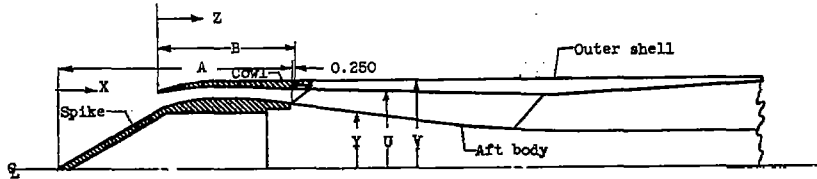
Lewis Flight Propulsion Laboratory  
National Advisory Committee for Aeronautics  
Cleveland, Ohio

#### REFERENCES

1. Cortright, Edgar M., Jr., and Connors, James F.: Survey of Some Preliminary Investigations of Supersonic Diffusers at High Mach Numbers. NACA RM E52E20, 1952.
2. Kantrowitz, Arthur, and Donaldson, Coleman duP.: Preliminary Investigation of Supersonic Diffusers. NACA ACR L5D20, 1945.
3. Ferri, Antonio: Application of the Method of Characteristics to Supersonic Rotational Flow. NACA Rep. 841, 1946. (Supersedes NACA TN 1135.)

- ~~CONFIDENTIAL~~
4. Preston, J. H.: The Boundary-Layer Flow over a Permeable Surface through which Suction is Applied. R. & M. No. 2244, British A.R.C., Feb. 1946.
  5. Connors, James F., and Woollett, Richard R.: Some Observations of Flow at the Throat of a Two-Dimensional Diffuser at a Mach Number of 3.85. NACA RM E52I04, 1952.
  6. Connors, James F., and Woollett, Richard R.: Experimental Investigation of a Two-Dimensional Split-Wing Ram-Jet Inlet at Mach Number of 3.85. NACA RM E52F04, 1952.
  7. Ferri, Antonio, and Nucci, Louis M.: The Origin of Aerodynamic Instability of Supersonic Inlets at Subcritical Conditions. NACA RM L50K30, 1951.
  8. Sibulkin, Merwin: Theoretical and Experimental Investigation of Additive Drag. NACA RM E51B13, 1951.

TABLE I - INLET DIMENSIONS



Aft body		Outer shell		
X	Y	Z	U	V
A	1.82	B	2.50	2.50
↓	Straight	↓	Straight	Cylind-
A + 4.50	taper	1.22	taper	rical
↓	1.731	B + 7.186	2.06	1 in.
A + 9.13	2.00	↓	rad. arc	
↓	Straight	B + 7.625	2.085	
A + 14.25	cylinder	↓	Straight	
	2.00	B + 12.75	taper	
			2.375	2.50

A length of spike from tip to point of attachment to aft body, in.

B length of cowl from lip to point of attachment to outer shell, in.



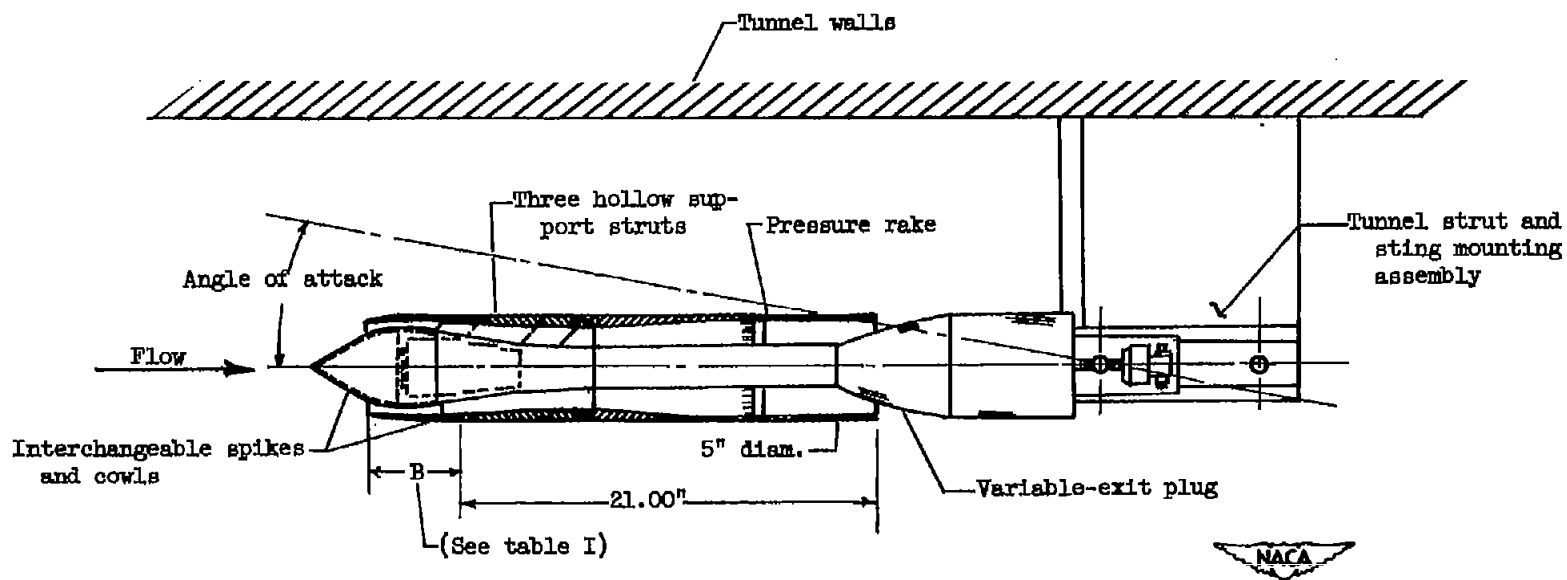
1 cone				
Spike (A, 6.370)		Cowl (B, 3.750)		
X	Y	Z	U	V
0	0	0	2.132	2.152
↓	Straight	.100	2.188	2.211
3.000	1.731	.200	2.223	2.262
3.100	1.782	.400	2.278	2.347
3.200	1.824	.600	2.318	2.411
3.400	1.887	.800	2.345	2.454
3.600	1.926	1.000	2.375	2.500
3.800	1.948	1.500	2.373	Cylind-
4.000	1.958	1.750	2.368	rical
4.200	1.960	2.000	2.360	↓
4.500	1.955	↓	Straight	
4.690	1.947	↓	taper	
5.000	1.930	5.750	2.300	↓
5.500	1.898			2.500
6.000	1.860			
6.370	1.820			

1 cone (low-angle cowl)				
Spike (A, 7.10)		Cowl (B, 4.287)		
X	Y	Z	U	V
0	0	0	2.500	2.500
↓	Straight	.200	2.560	Straight
3.292	1.922	1.902	2.860	taper
4.082	1.902	1.902	↓	2.500
4.500	1.888	1.888	↓	Cylind-
5.000	1.890	4.288	2.300	rical
5.500	1.880			2.500
6.000	1.870			
6.300	1.862			
6.800	1.842			
7.100	1.820			

2 cone				
Spike (A, 9.852)		Cowl (B, 5.750)		
X	Y	Z	U	V
0	0	0	2.165	2.165
↓	Straight	.100	2.205	2.219
3.802	1.384	.200	2.239	2.266
↓	Straight	.300	2.269	2.316
4.452	1.834	.400	2.295	2.358
4.552	1.902	.500	2.530	2.419
4.652	1.953	1.000	2.364	2.483
4.752	1.993	1.250	2.372	2.497
4.952	2.054	1.500	2.375	2.500
5.152	2.095	↓	Cylin-	Cylin-
5.352	2.119	3.000	2.352	dri
5.602	2.133	3.250	2.372	↓
5.852	2.158	3.500	2.369	
6.102	2.136	3.750	2.365	
6.352	2.133	4.000	2.358	
6.852	2.116	5.750	2.300	↓
7.352	2.085			2.500
7.852	2.046			
8.352	1.997			
8.852	1.943			
9.352	1.883			
9.852	1.820			

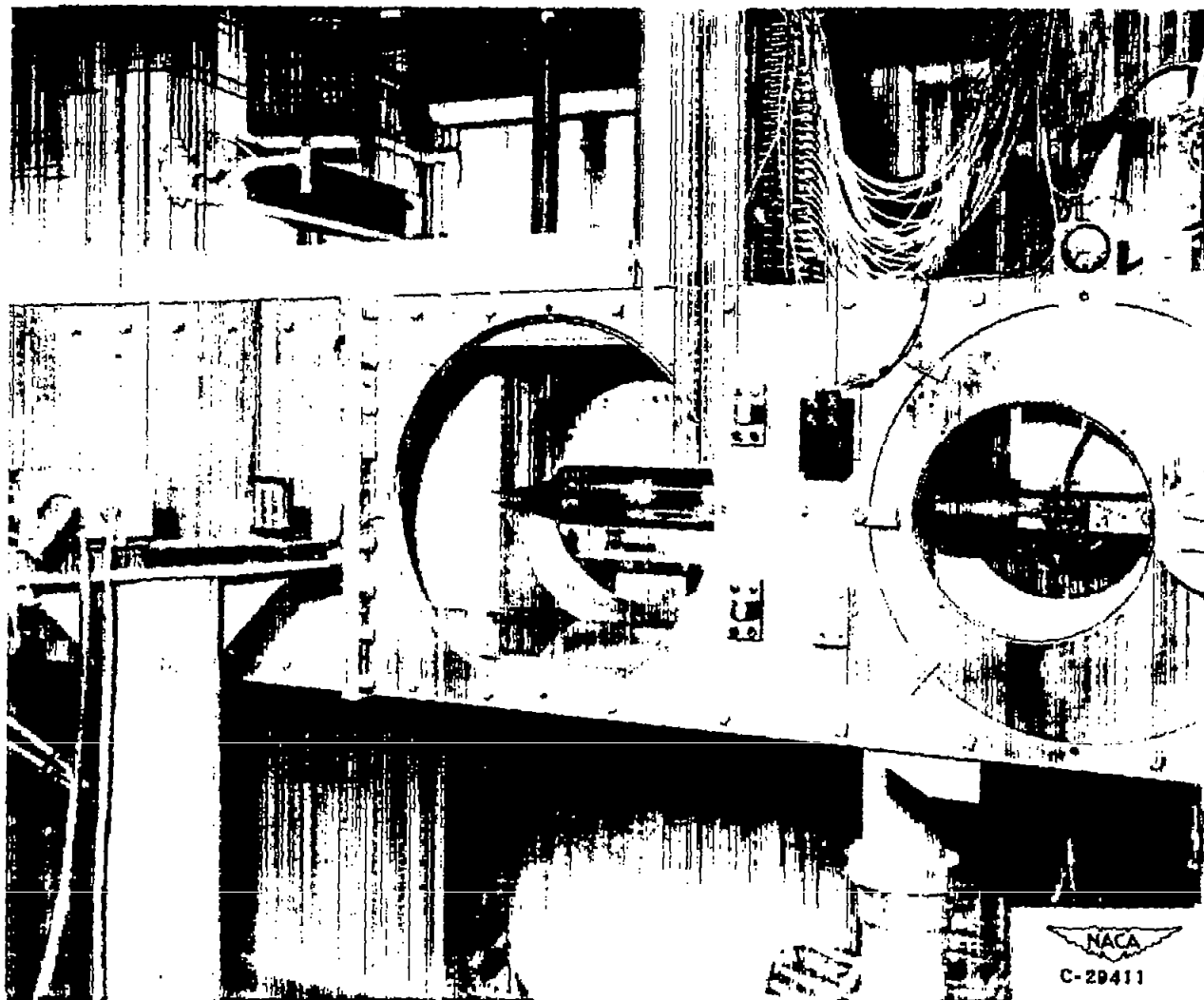
Isentropic				
Spike (A, 14.741)		Cowl (B, 7.750)		
X	Y	Z	U	V
0	0	0	2.240	2.240
.500	.075	.025	2.262	2.272
1.000	.145	.050	2.277	2.291
1.500	.216	.100	2.298	2.325
2.000	.284	.200	2.328	2.370
2.500	.357	.300	2.346	2.404
3.000	.436	.400	2.358	2.432
3.500	.528	.500	2.370	2.469
4.000	.624	.600	2.376	2.492
4.500	.742	1.000	2.378	2.500
5.000	.876	↓	Cylin-	Cylin-
5.500	1.031	↓	dri	rical
6.000	1.210	5.300	2.378	
6.500	1.433	5.500	2.376	
7.000	1.745	5.750	2.370	
7.100	1.830	6.000	2.360	
7.200	1.922	↓	Straight	
7.300	2.025	↓	taper	
7.400	2.100	7.750	2.300	↓
7.500	2.137			2.500
7.600	2.159			
7.700	2.170			
8.000	2.178			
8.250	2.180			
9.000	2.174			
9.188	2.170			
10.000	2.153			
11.000	2.113			
12.000	2.060			
13.000	1.994			
14.000	1.906			
14.741	1.820			

2644



(a) Schematic drawing of 5-inch ram-jet installation in 2- by 2-foot supersonic wind tunnel.

Figure 1. - Experimental model.



(b) Photograph showing model mounted in 2- by 2-foot supersonic wind tunnel.

Figure 1. - Continued. Experimental model.

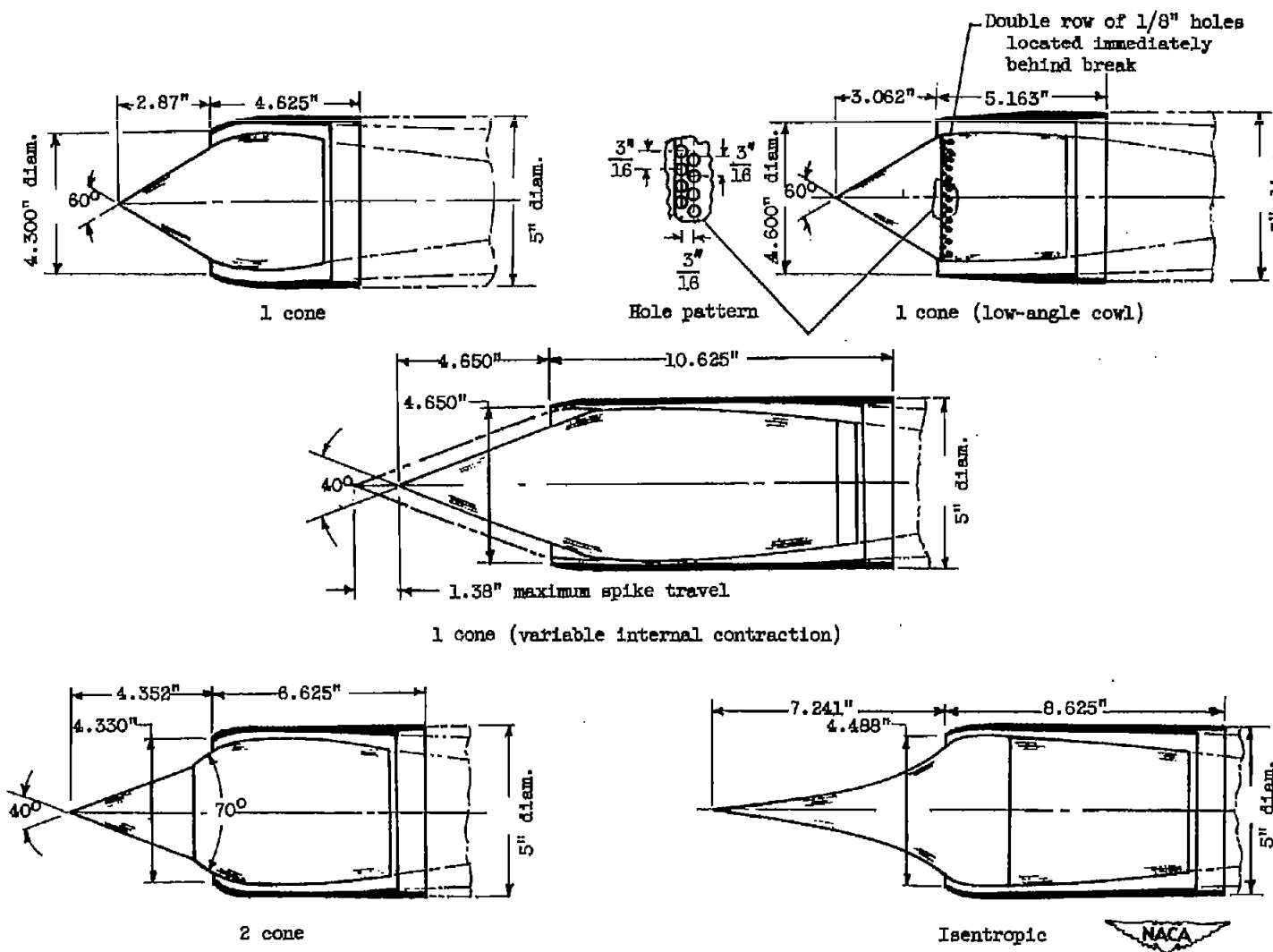
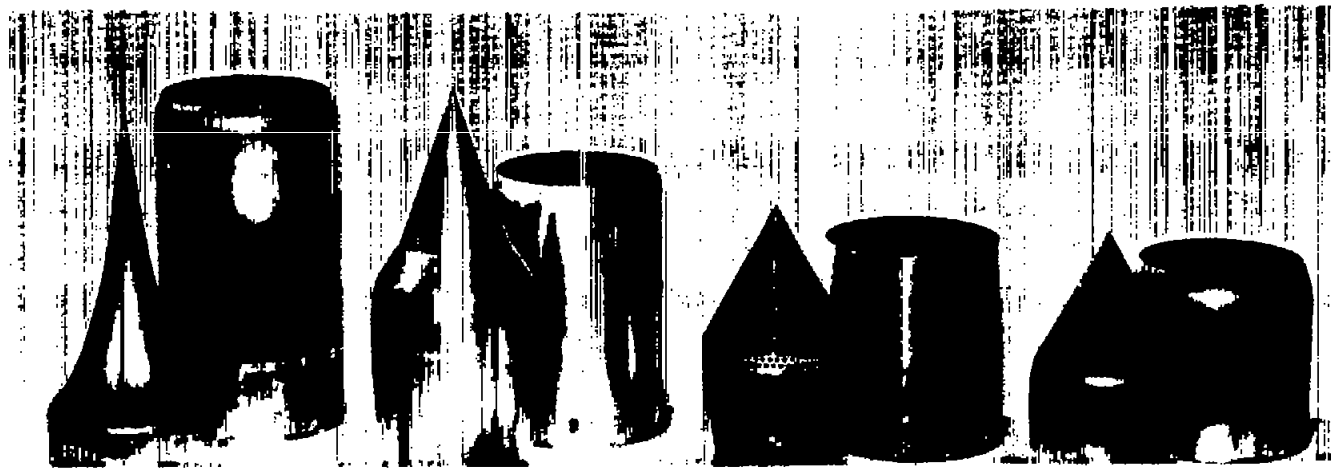
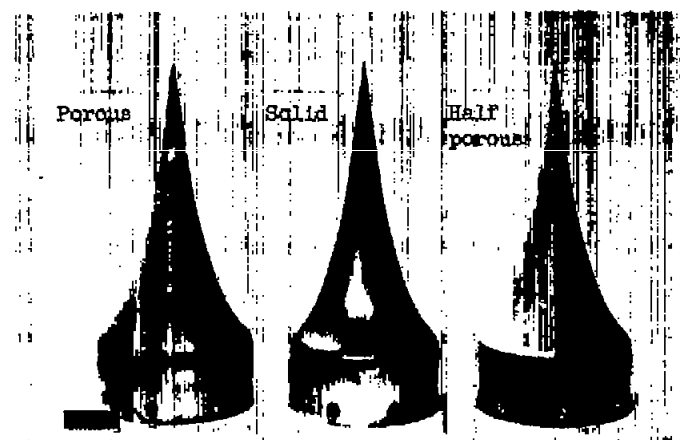


Figure 1. - Continued. Experimental model.



NACA  
C-29386



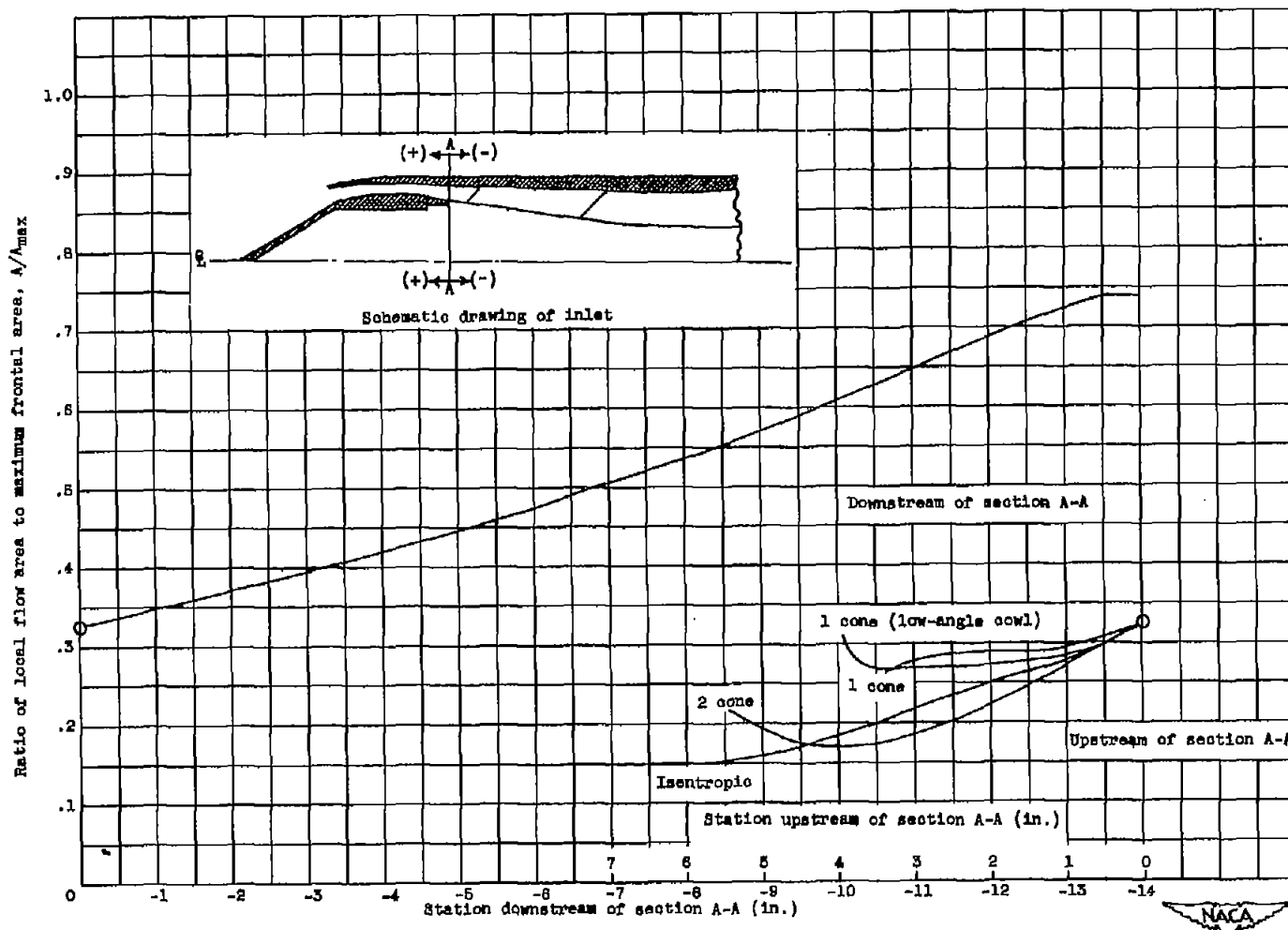
Isentropic spike variations

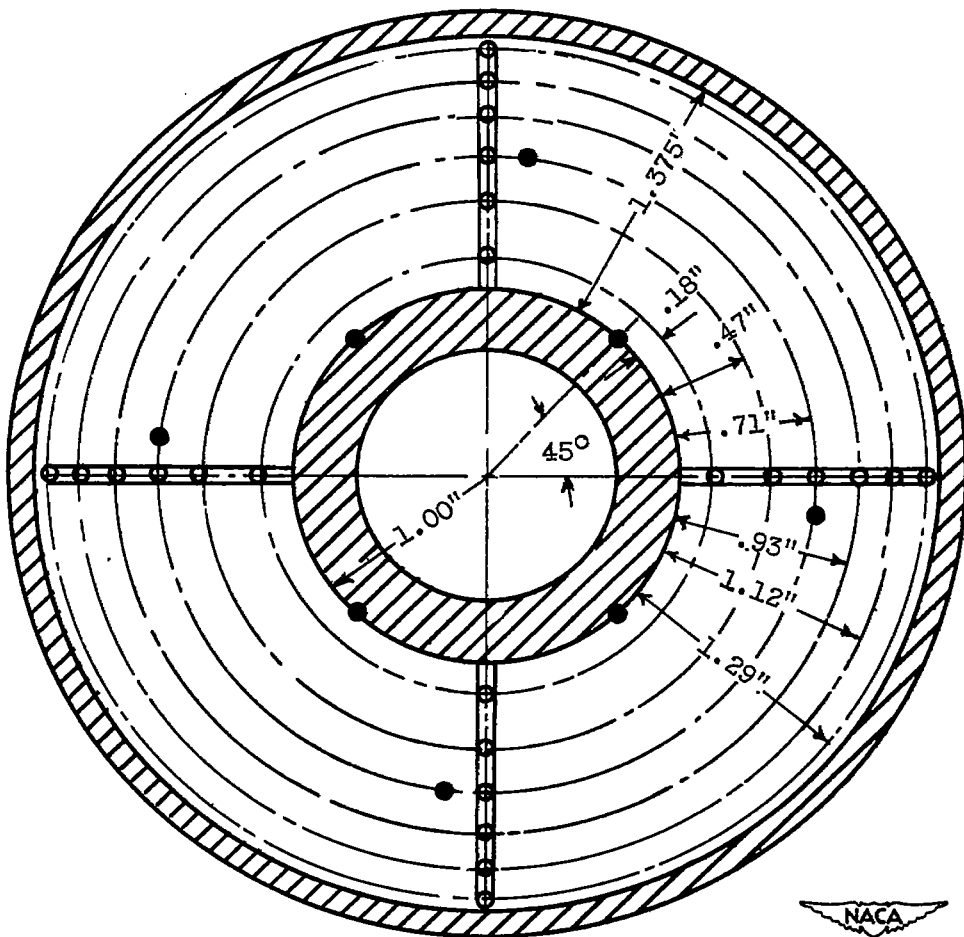
(d) Photographs of 5-inch ram-jet inlets.

NACA  
C-29388

Figure 1. - Continued. Experimental models.

NACA RM E521S

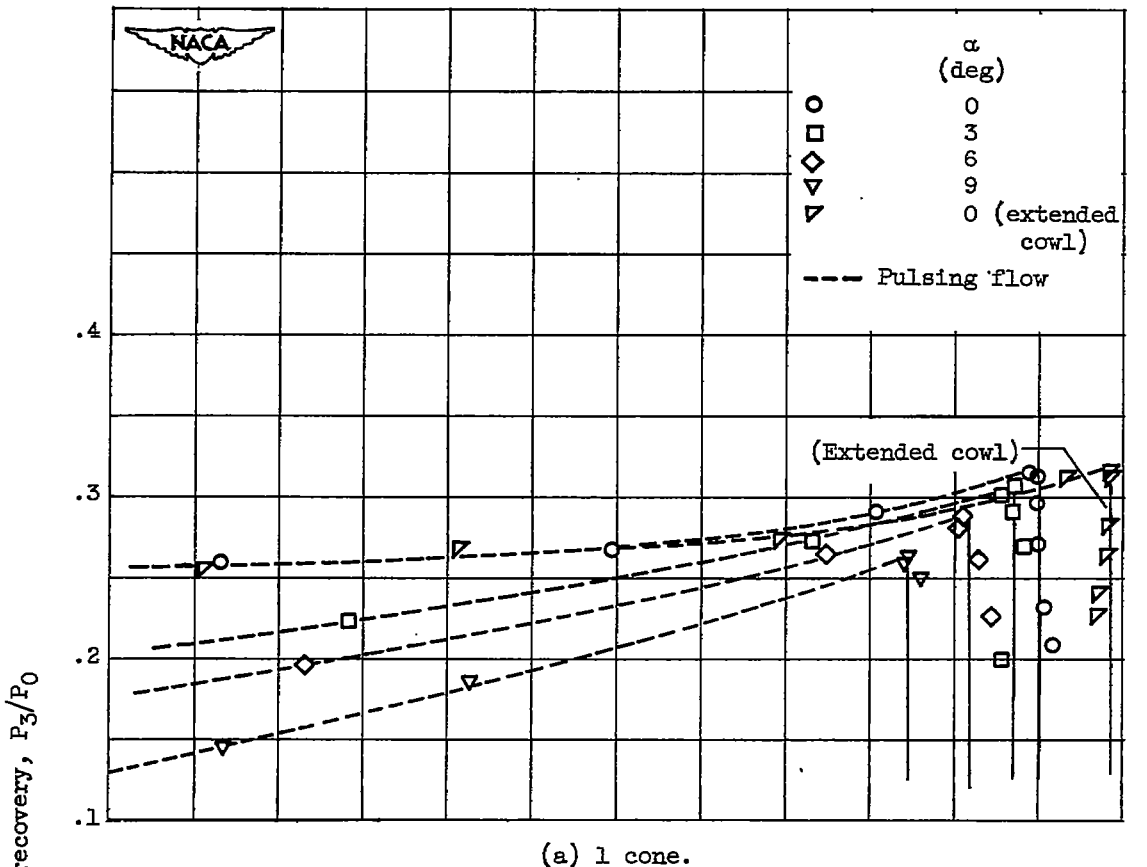




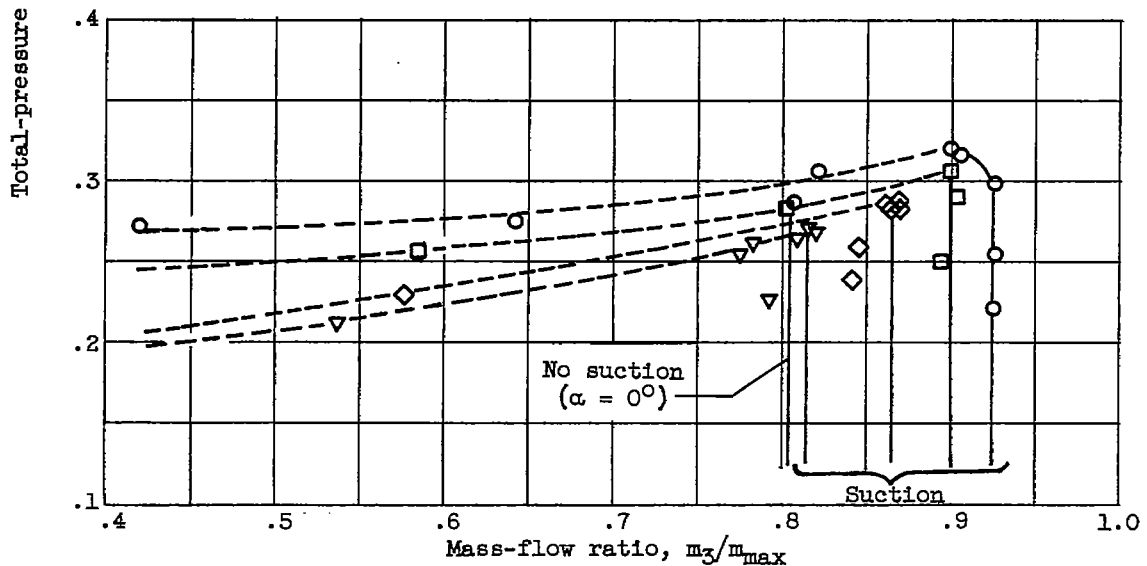
- Pitot tube
- Static orifice

(f) Instrumentation. Pressure-rake details.

Figure 1. - Concluded. Experimental model.



(a) 1 cone.



(b) 1 cone (low-angle cowl).

Figure 2. - Diffuser characteristics of 1-cone inlets for several angles of attack  $\alpha$ .

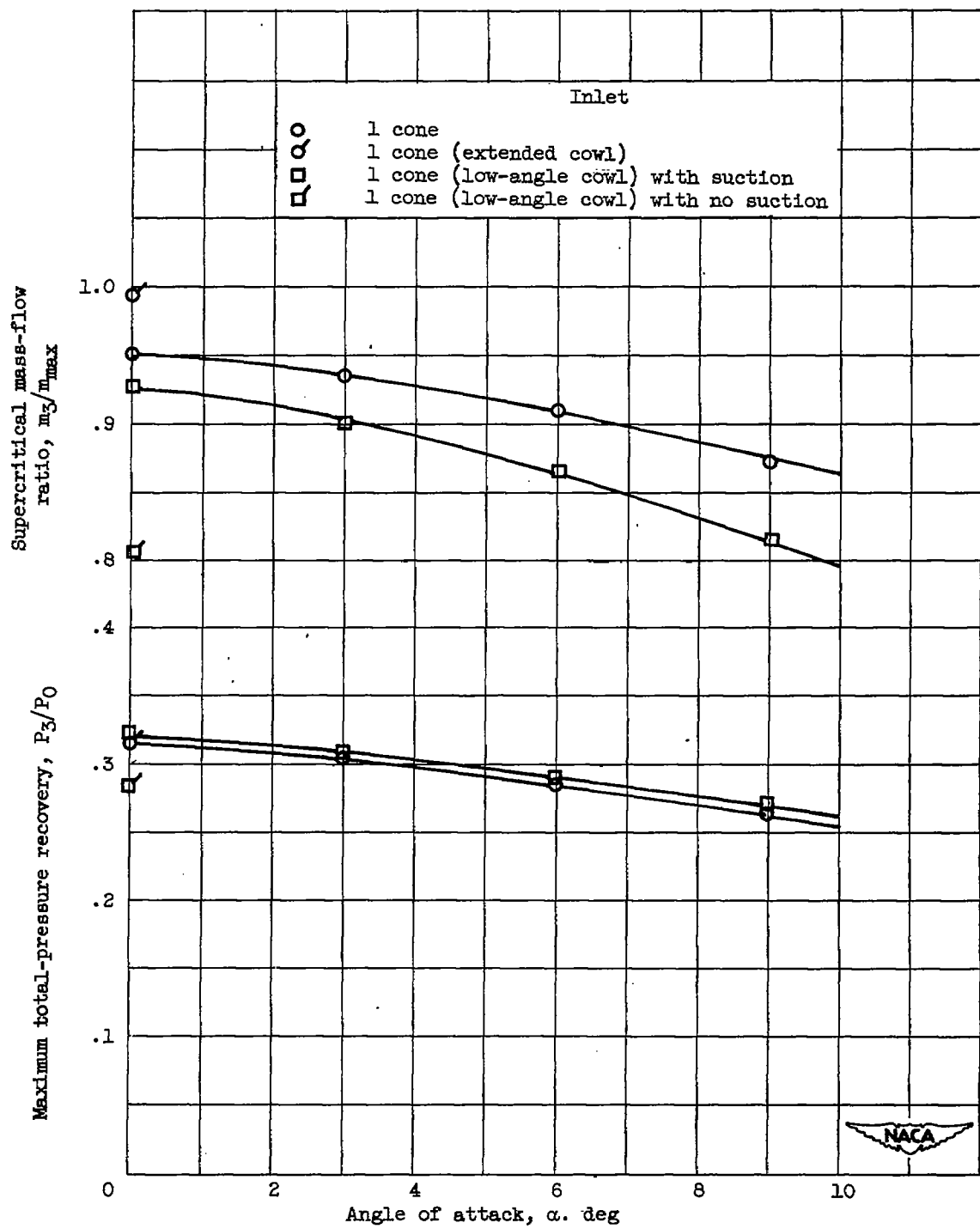


Figure 3. - Effect of angle of attack on performance of I-cone inlets.

2644

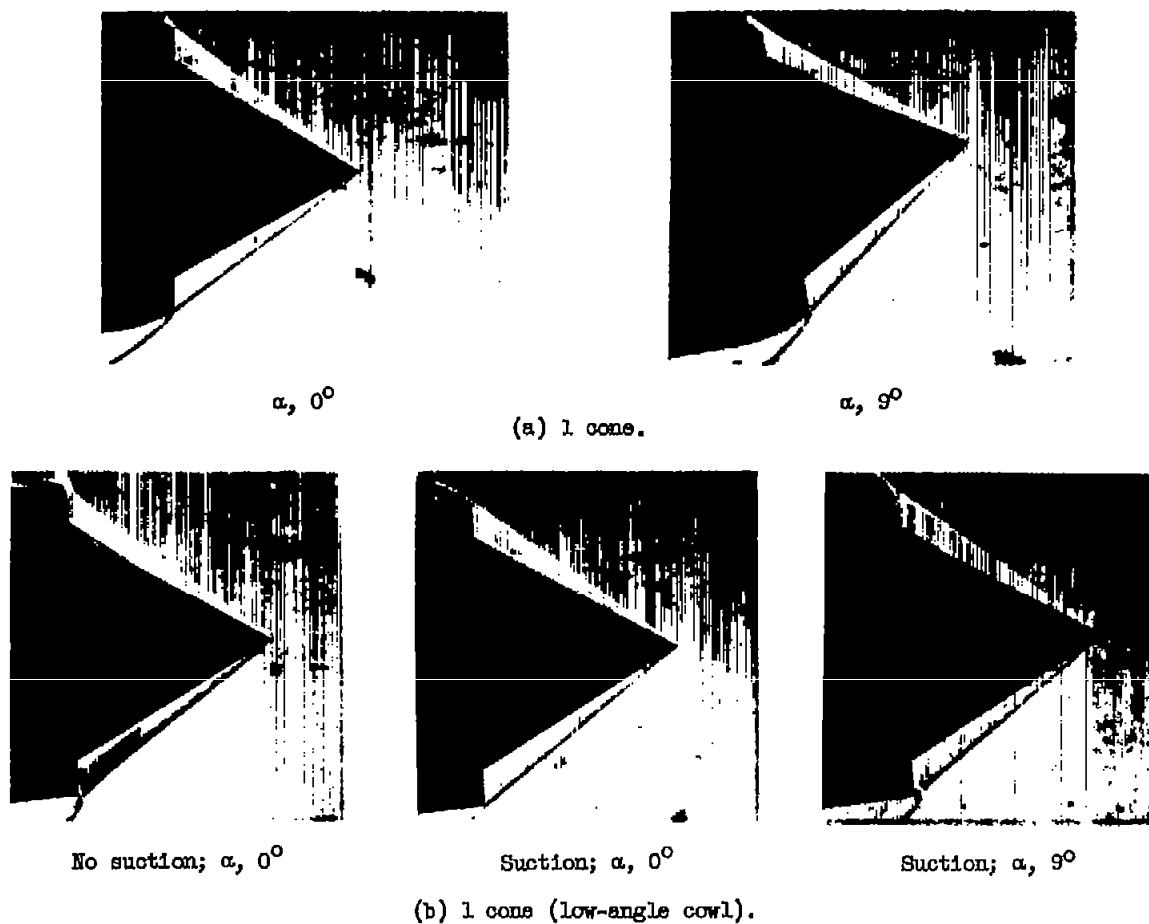


Figure 4. - Schlieren photographs of L-cone inlets at zero and  $9^{\circ}$  angles of attack  $\alpha$ .



CONFIDENTIAL



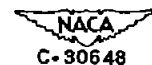
Tip projection, 5.466 inches;  
no suction.

Tip projection, 5.350 inches;  
no suction. (Unsteady flow.)

Tip projection, 4.859 inches;  
local suction on cone.

(c) 1 cone (variable internal contraction).

Figure 4. - Concluded. Schlieren photographs of 1-cone inlets at zero and  $9^{\circ}$  angles of attack  $\alpha$ .



NACA RM E52115

2644

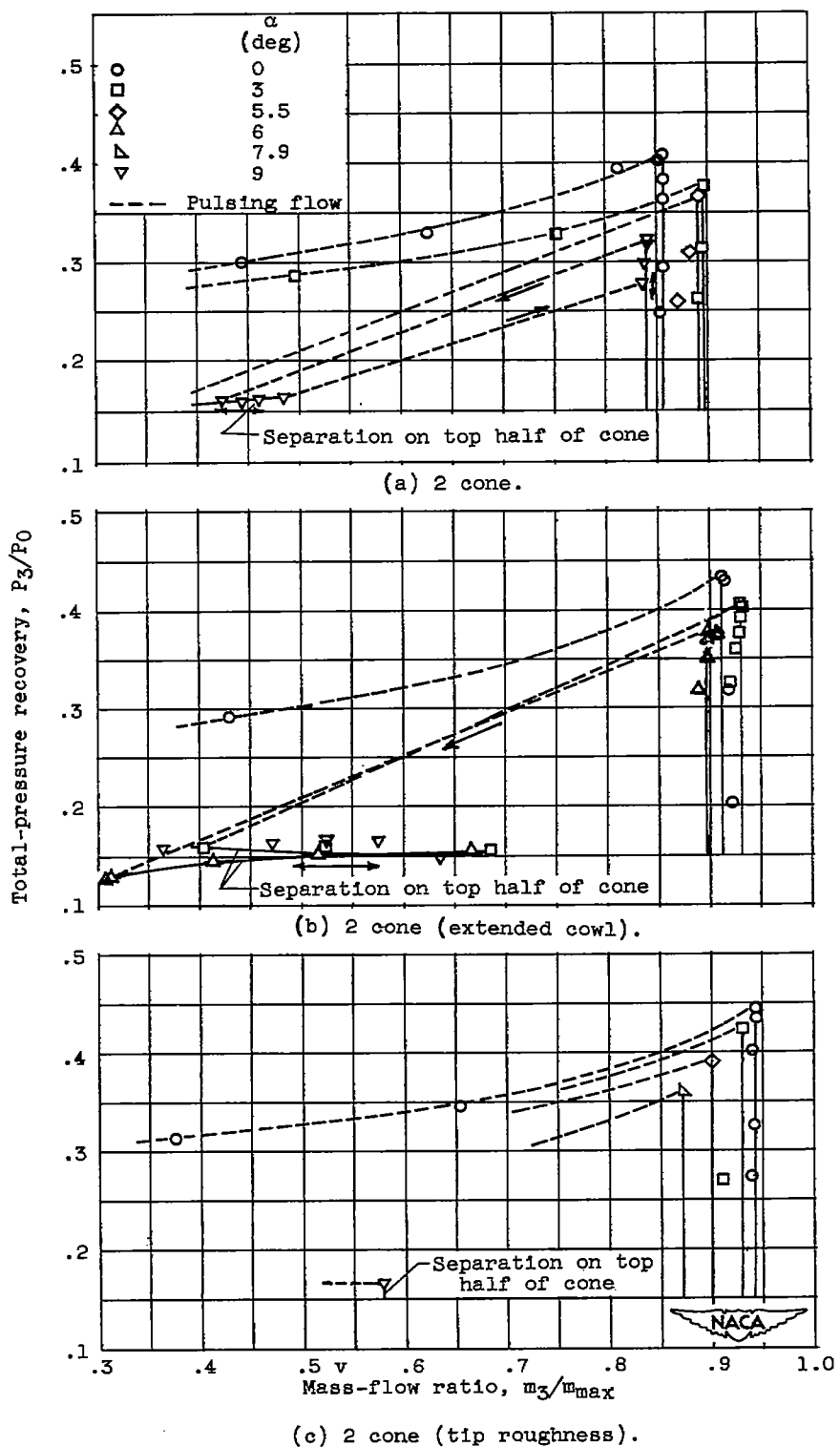


Figure 5. - Diffuser characteristics of 2-cone inlets for several angles of attack  $\alpha$ .

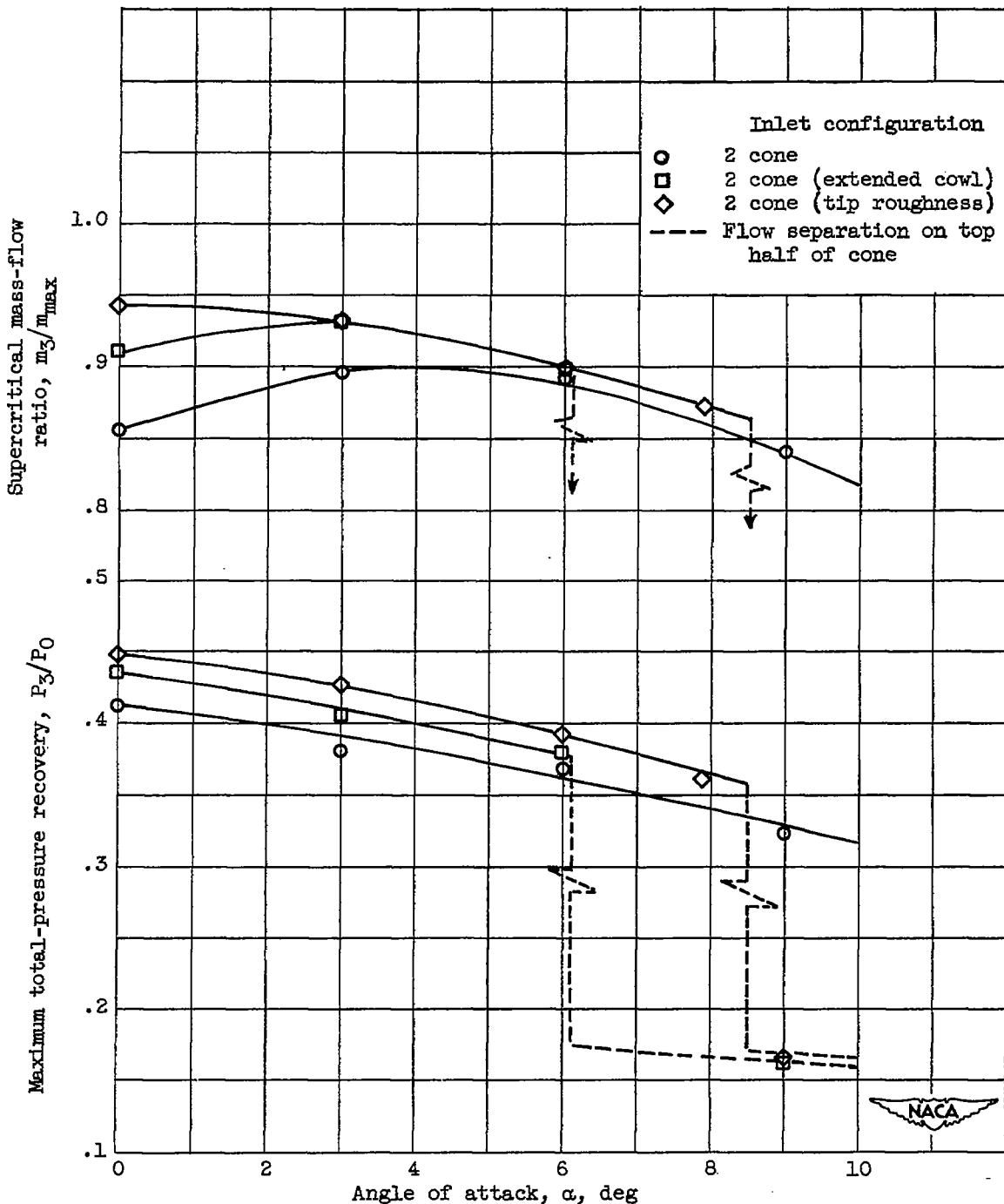
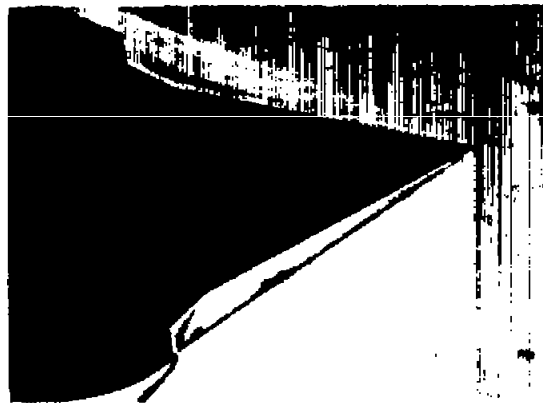
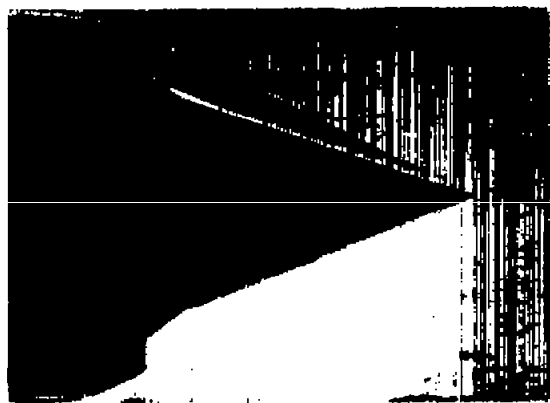


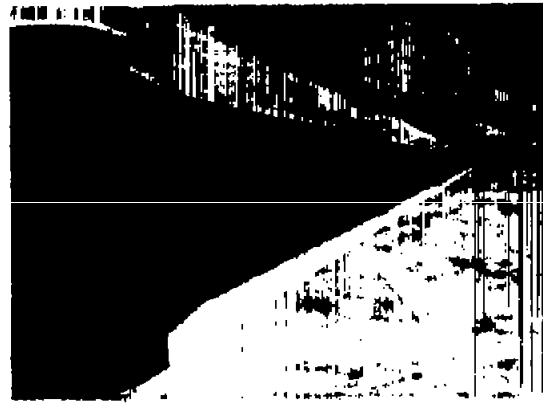
Figure 6. - Effect of angle of attack on performance of 2-cone inlets.

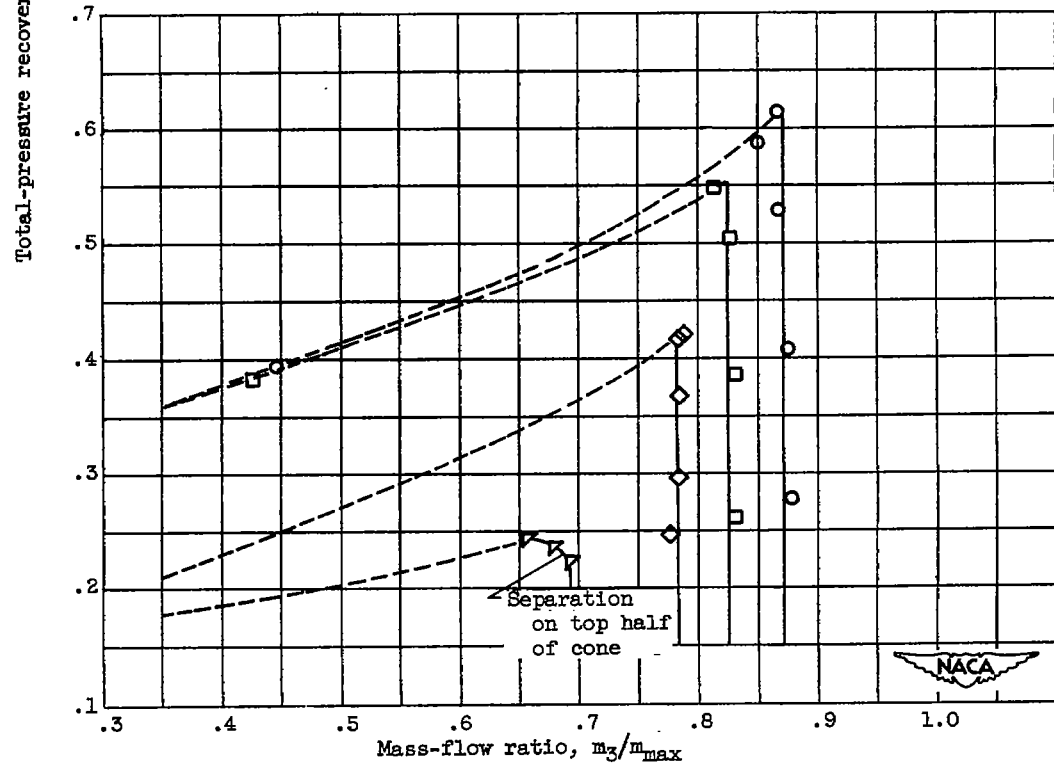
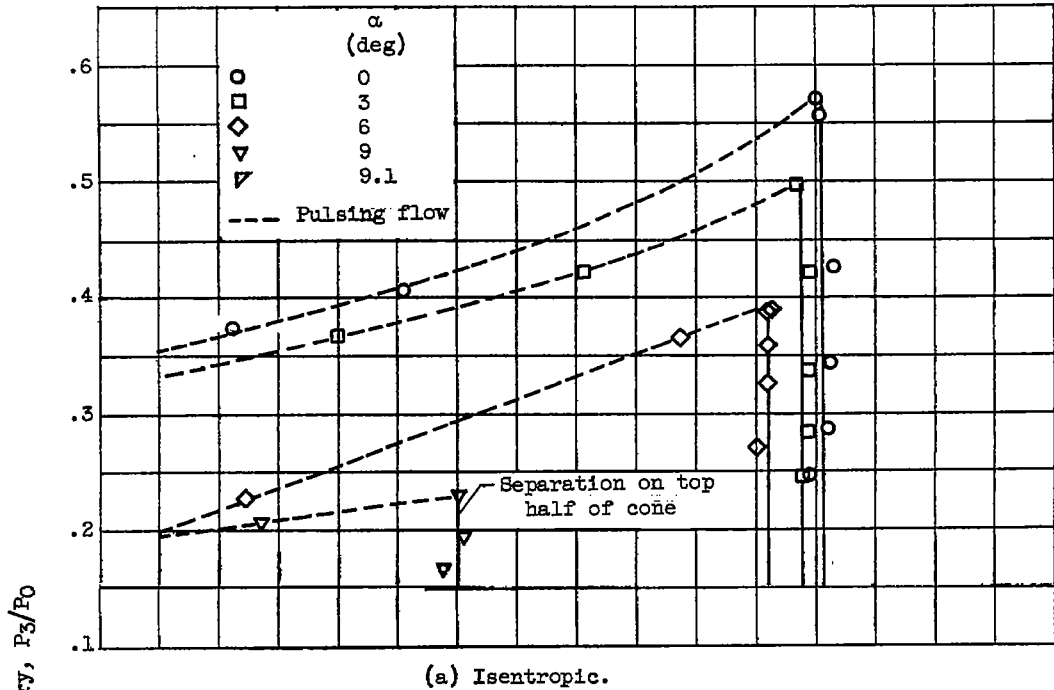
 $\alpha, 0^\circ$  $\alpha, 90^\circ$ 

(a) 2 cone.

 $\alpha, 0^\circ$ 

(b) 2 cone (tip roughness).

 $\alpha, 90^\circ$ Figure 7. - Schlieren photographs of 2-cone inlets at zero and  $90^\circ$  angles of attack  $\alpha$ .



(b) Isentropic (tip roughness).

Figure 8. - Diffuser characteristics of isentropic inlets for several angles of attack  $\alpha$ .

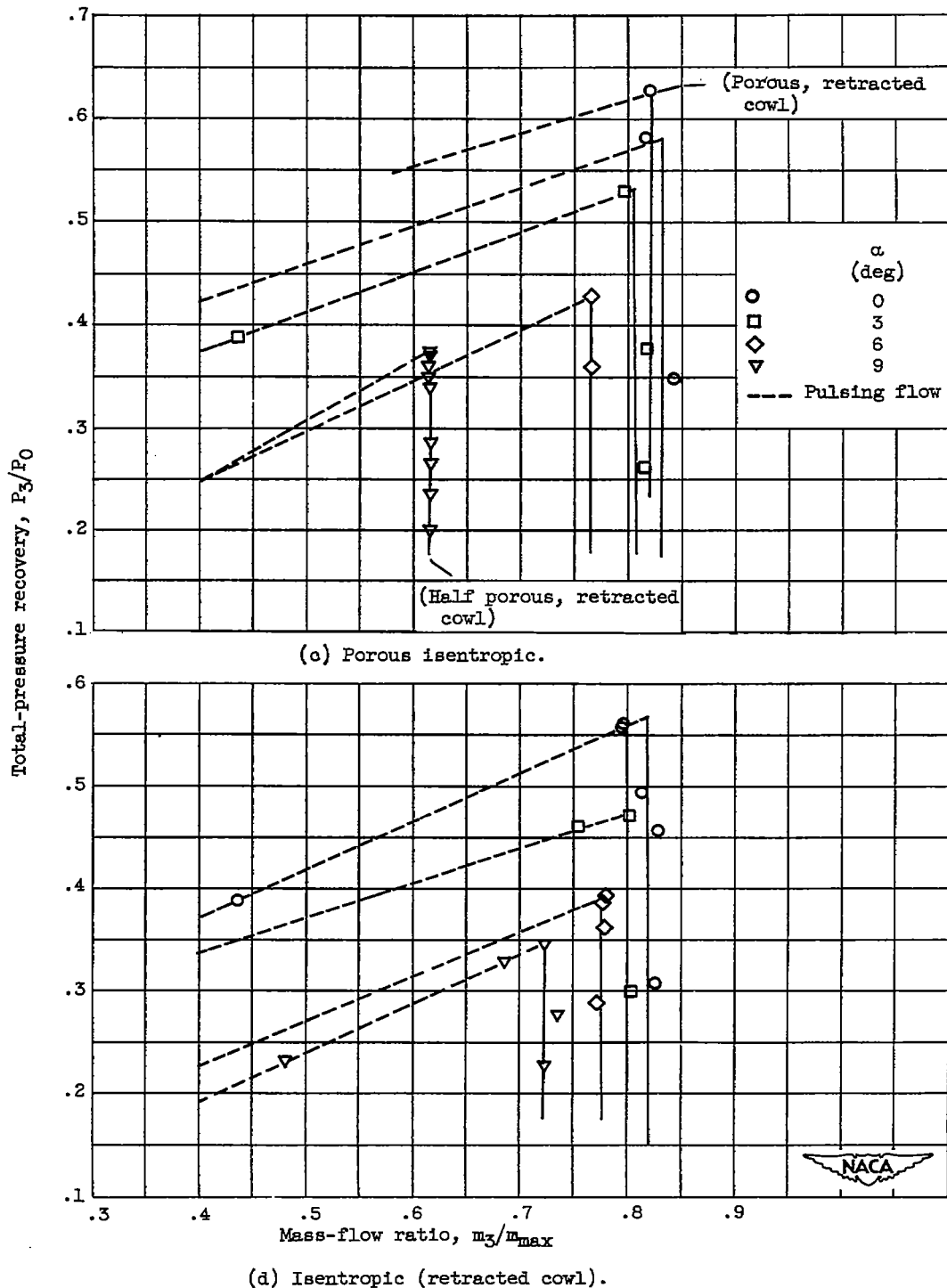


Figure 8. - Concluded. Diffuser characteristics of isentropic inlets for several angles of attack  $\alpha$ .

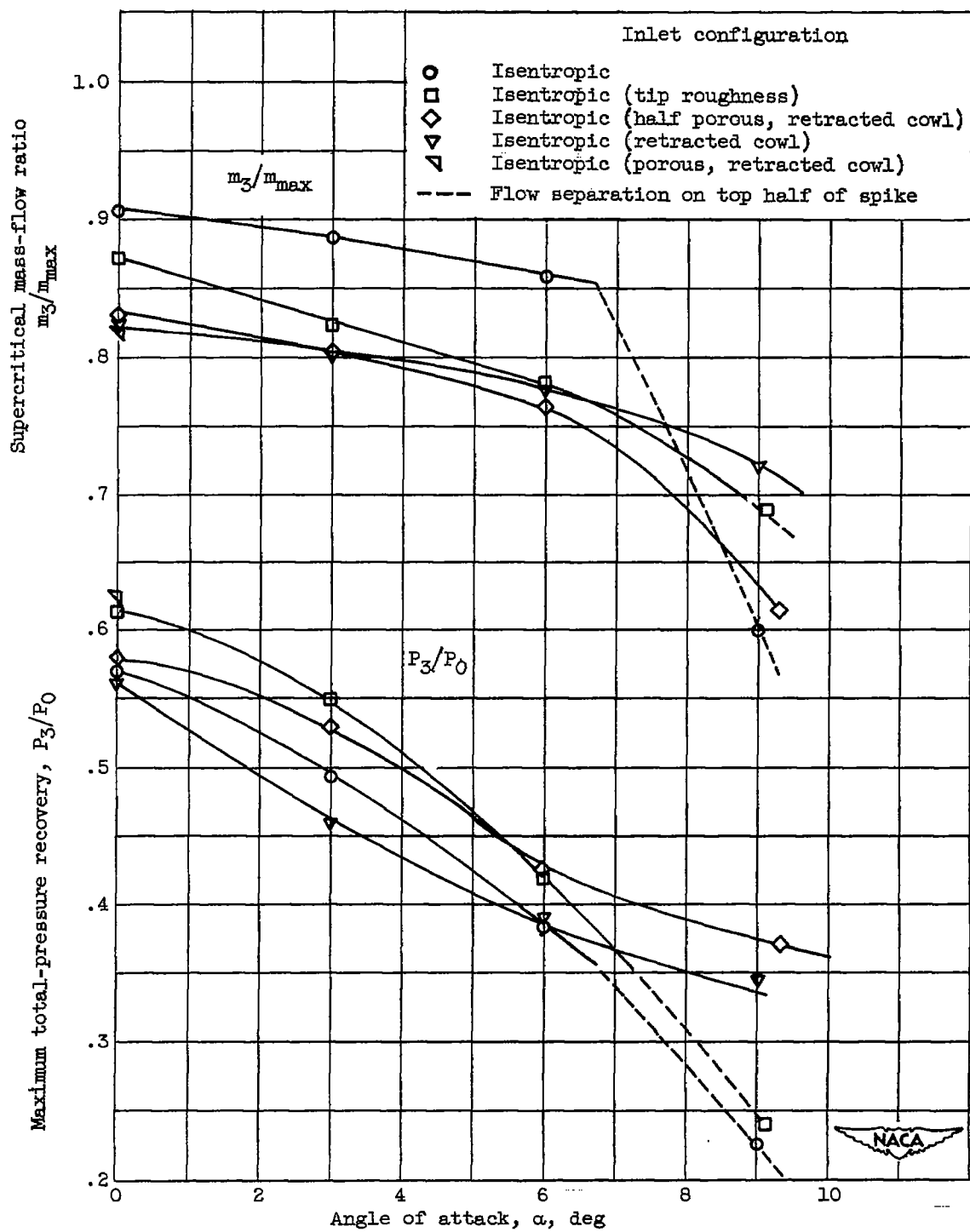


Figure 9. - Effect of angle of attack on performance of isentropic inlets.

2644

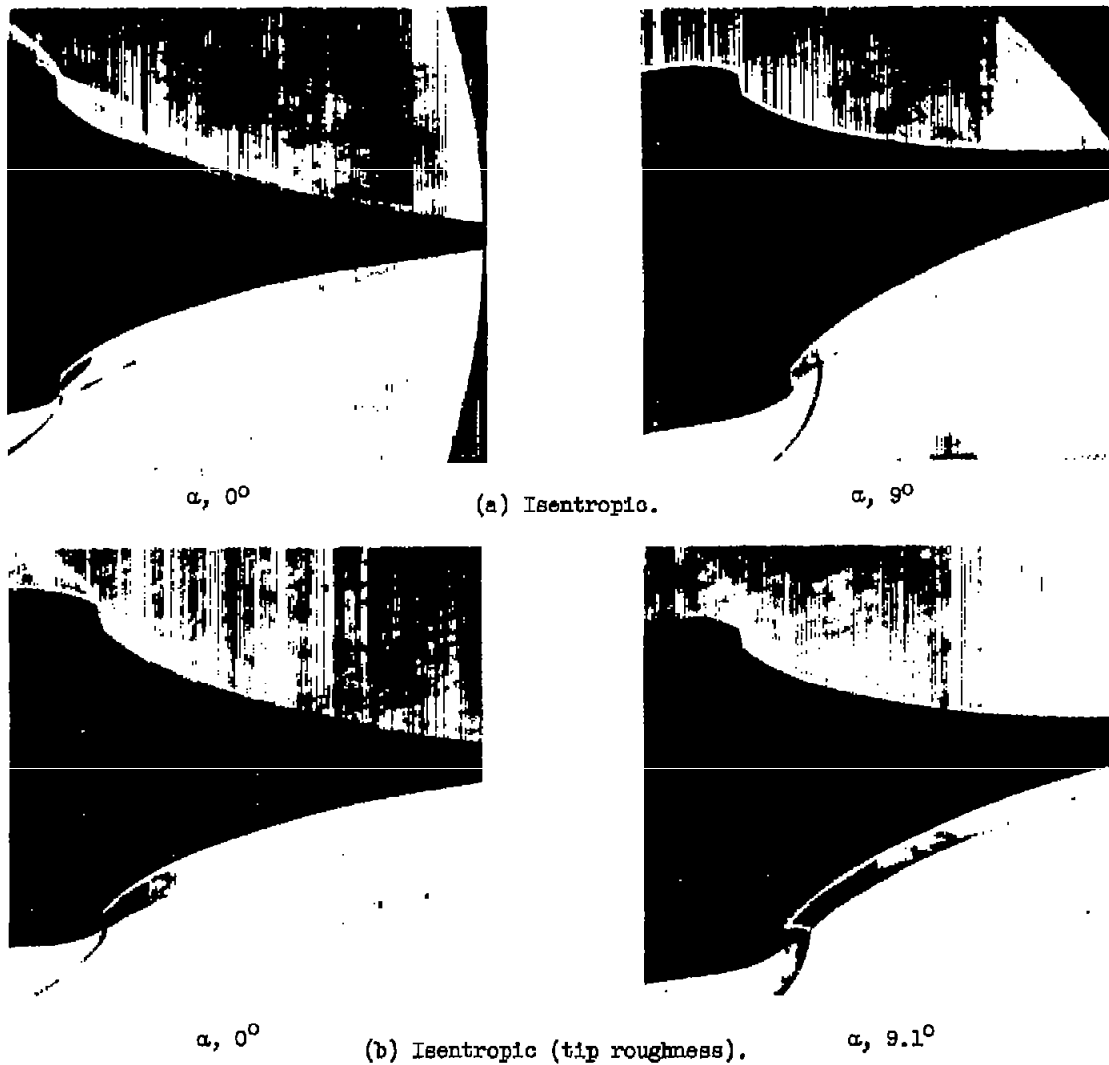
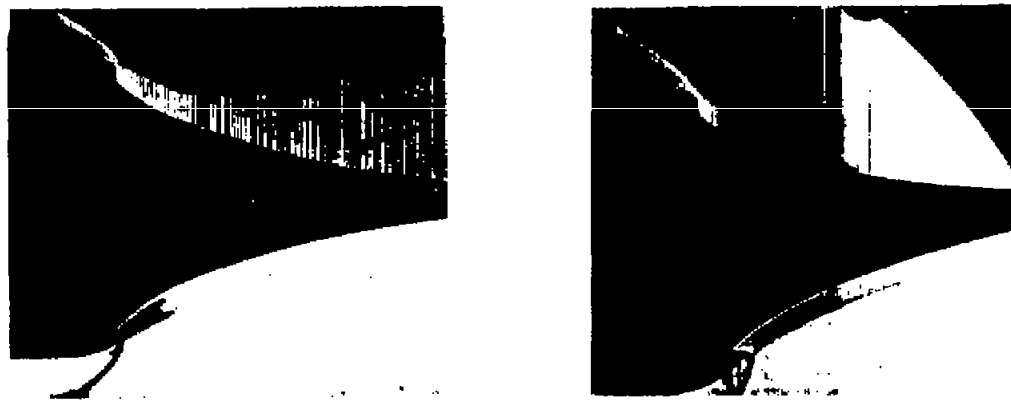
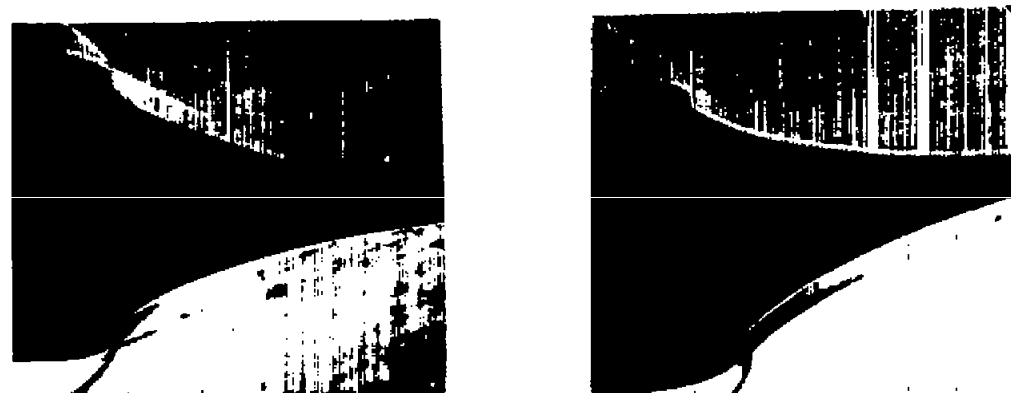


Figure 10. - Schlieren photographs of isentropic inlets at zero and approximately  $9^\circ$  angles of attack  $\alpha$ .



(c) Isentropic (half porous, retracted cowl).



(d) Isentropic (retracted cowl).



Figure 10. - Concluded. Schlieren photographs of isentropic inlets at zero and approximately  $9^\circ$  angles of attack  $\alpha$ .

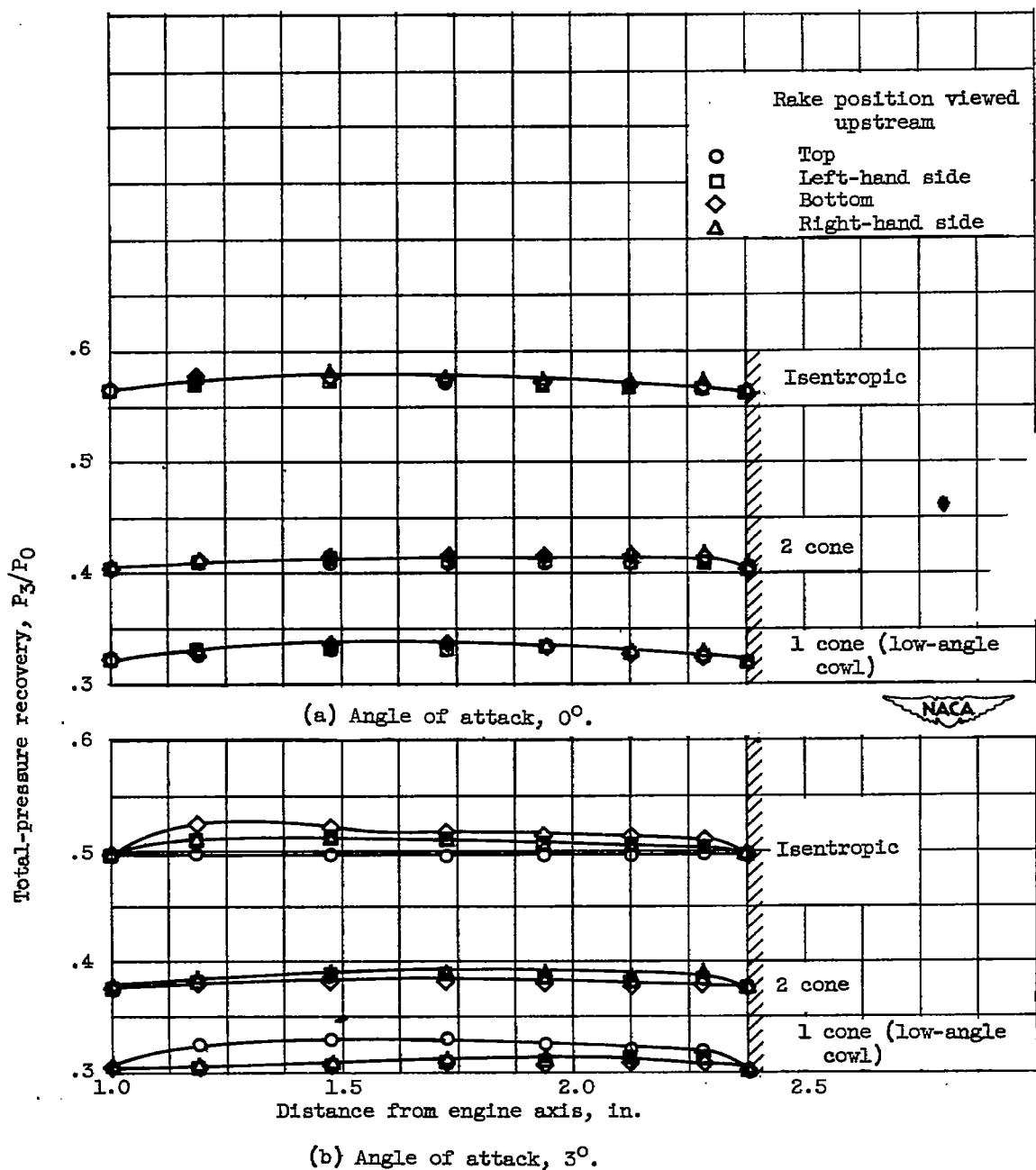


Figure 11. - Total-pressure profiles obtained during critical operation for several angles of attack.

2644

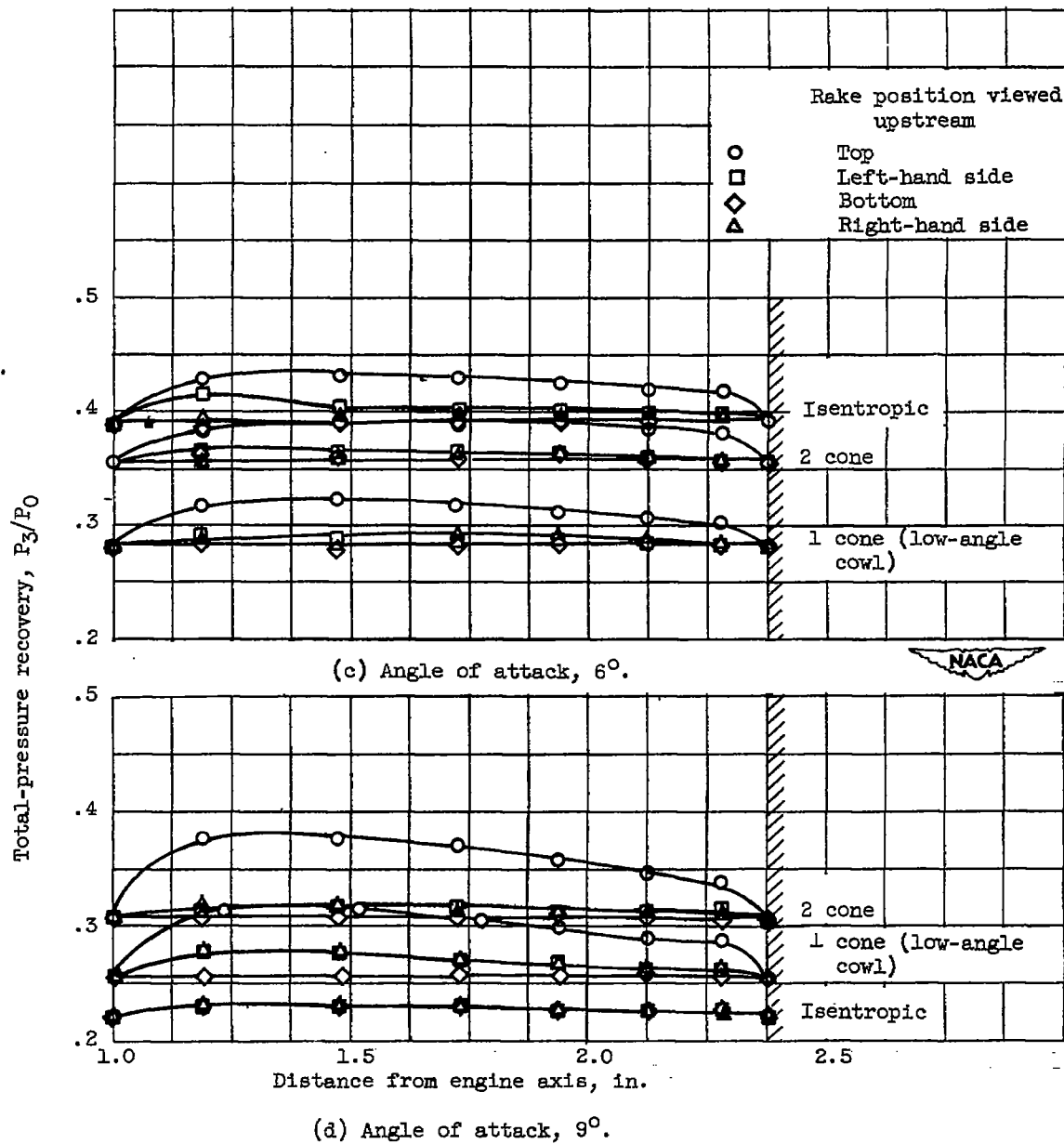
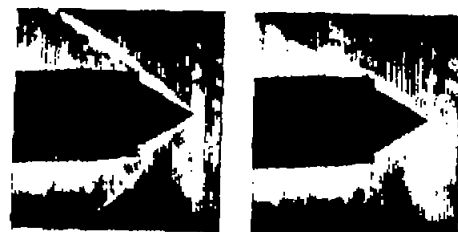


Figure 11. - Concluded. Total-pressure profiles obtained during critical operation for several angles of attack.



(a) Angle of attack,  $0^{\circ}$ ; approximate frequency,  
73 cycles per second.

NACA  
C-29561



(b) Angle of attack, 6.10; approximate frequency,  
59 cycles per second.

Figure 12. - Selected high-speed photographs showing variation of inlet flow pattern during pulsing subcritical operation of 1-cowl (low-angle cowl) inlet.



(a) Angle of attack,  $0^{\circ}$ ; approximate frequency, 36 cycles per second.



(b) Angle of attack,  $5.2^{\circ}$ ; approximate frequency, 18 cycles per second.

NACA  
C-29562

Figure 13. - Selected high-speed photographs showing variation of inlet flow pattern during pulsing subcritical operation of isentropic inlet.

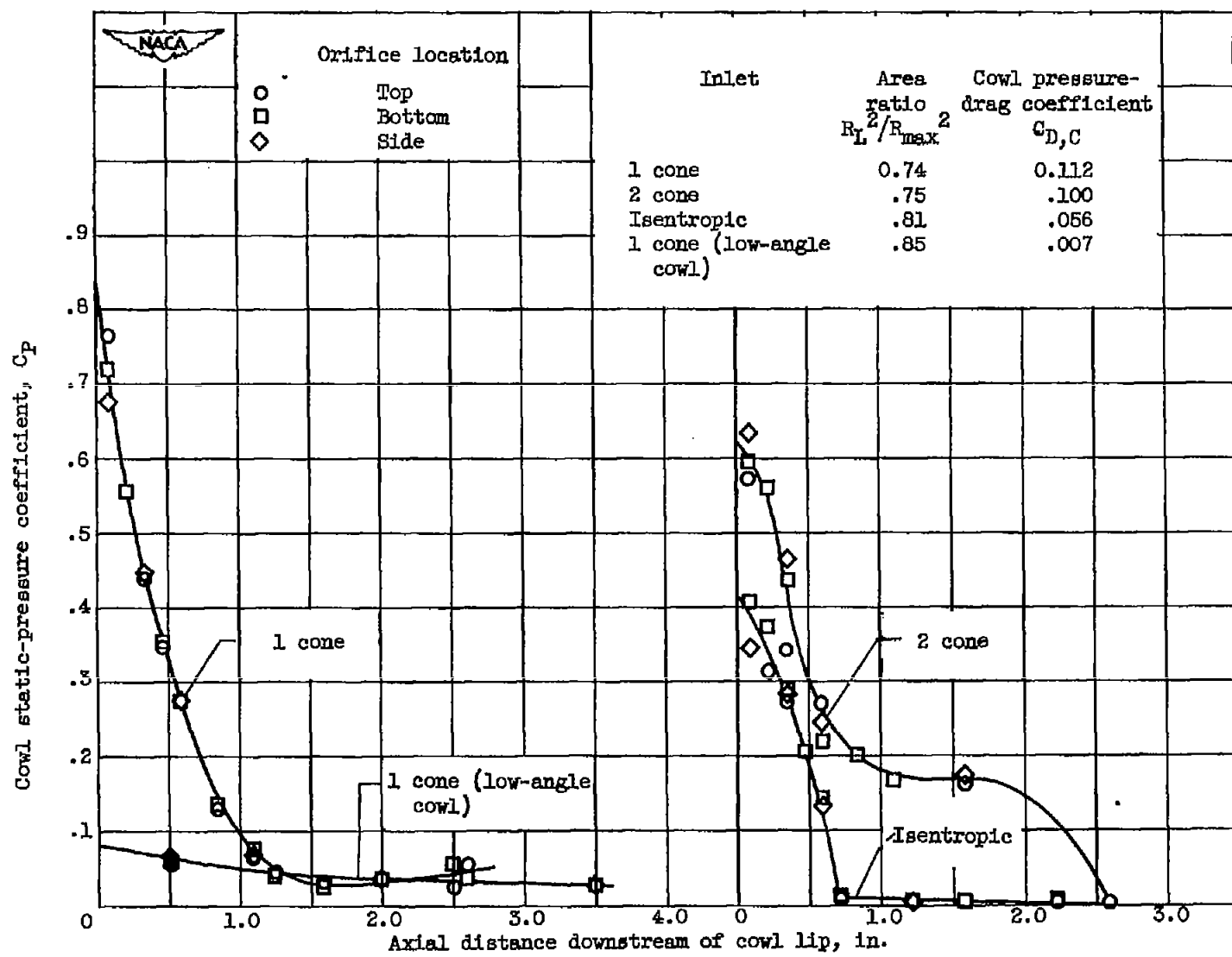


Figure 14. - Cowl pressure distributions at zero angle of attack.

CONFIDENTIAL

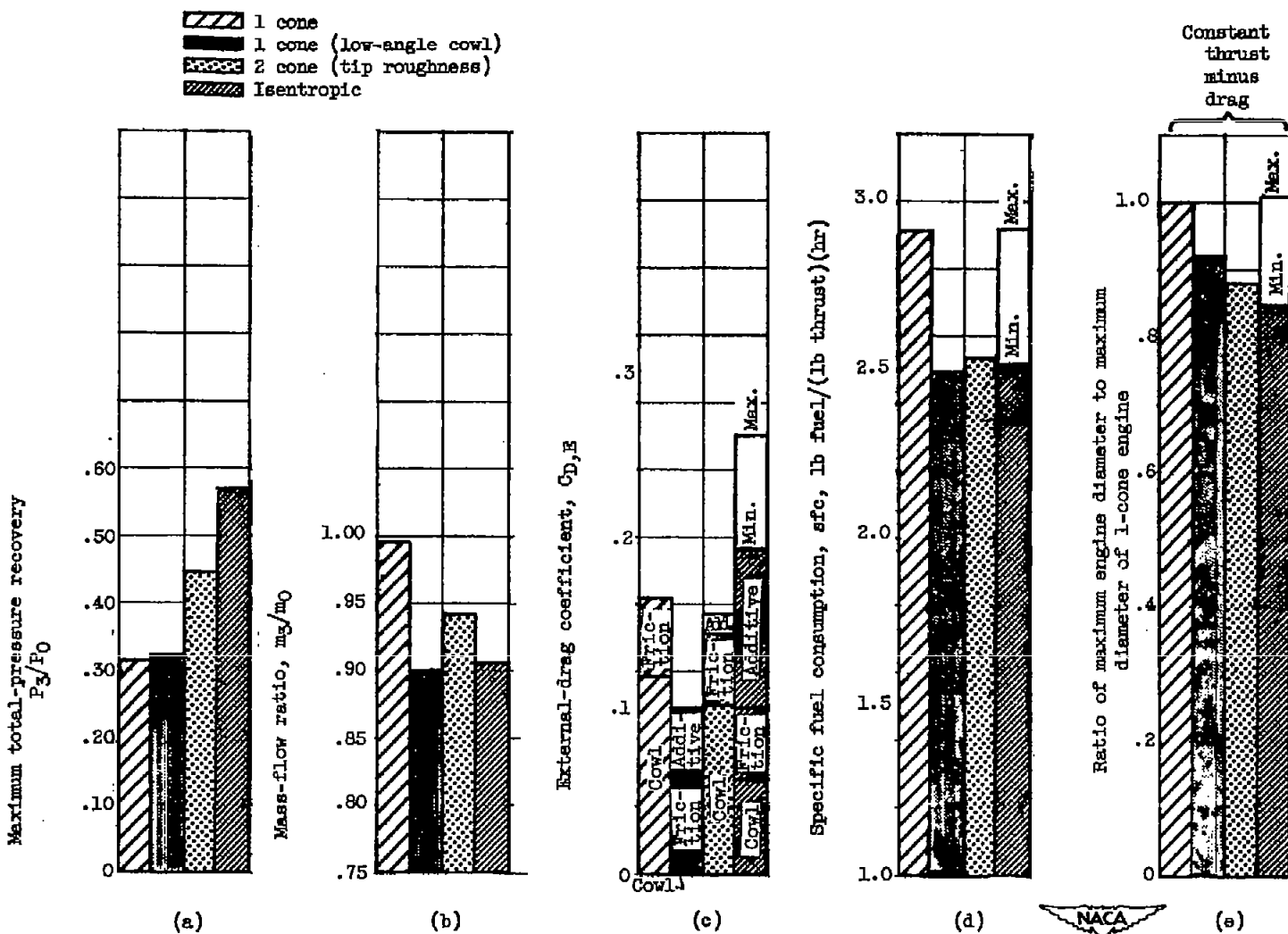


Figure 15. - Comparative performance parameters obtained with specific inlet configurations applied to hypothetical ram-jet engines. Mach number, 3.85; altitude, 80,000 feet; fuel-air ratio, 0.024; combustion efficiency, 0.90.